Report PME-FM-92-1

INJECTION OF DRAG-REDUCING ADDITIVES INTO TURBULENT WATER FLOWS

Investigation of laser-induced fluorescence for concentration measurements

Andreas C. Schwarz and William G. Tiederman
School of Mechanical Engineering
Purdue University
West Lafayette, Indiana 47907-1288

Dec.
[redacted]y 1992

Final Report for Period 01 December 1990 - 15 May 1992

Approved for public release, distribution unlimited

Prepared for

OFFICE OF NAVAL RESEARCH
800 North Quincy Street
Arlington, VA 22217-5000

SECURITY CLASSIFICATION OF THIS PAGE (When Data Entered)

REPORT DOCUMENTATION PAGE

READ INSTRUCTIONS BEFORE COMPLETING FORM

1. REPORT NUMBER: PME-FM-92-1	2. GOVT ACCESSION NO.: –
3. RECIPIENT'S CATALOG NUMBER: –	
4. TITLE (and Subtitle): INJECTION OF DRAG-REDUCING ADDITIVES INTO TURBULENT WATER FLOWS - Investigation of laser-induced fluorescence for concentration measurement	5. TYPE OF REPORT & PERIOD COVERED: – –
	6. PERFORMING ORG. REPORT NUMBER: –
7. AUTHOR(s): Andreas C. Schwarz, William G. Tiederman	8. CONTRACT OR GRANT NUMBER(s): N00014-91-J-1446
9. PERFORMING ORGANIZATION NAME AND ADDRESS: School of Mechanical Engineering Purdue University West Lafayette, IN 47907-1288	10. PROGRAM ELEMENT, PROJECT, TASK AREA & WORK UNIT NUMBERS: 4322754--08
11. CONTROLLING OFFICE NAME AND ADDRESS: Office of Naval Research 800 North Quincy Street Arlington, VA 22217-5000	12. REPORT DATE: December, 1992
	13. NUMBER OF PAGES: 58
14. MONITORING AGENCY NAME & ADDRESS (if different from Controlling Office): –	15. SECURITY CLASS. (of this report): –
	15a. DECLASSIFICATION/DOWNGRADING SCHEDULE

16. DISTRIBUTION STATEMENT (of this Report)

Approved for Public Release: Distribution Unlimited

17. DISTRIBUTION STATEMENT (of the abstract entered in Block 20, if different from Report)

18. SUPPLEMENTARY NOTES

19. KEY WORDS (Continue on reverse side if necessary and identify by block number)

Laser-induced fluorescence, Turbulent boundary layers, Wall injection

20. ABSTRACT (Continue on reverse side if necessary and identify by block number)

DD FORM 1 JAN 73 1473 EDITION OF 1 NOV 65 IS OBSOLETE
S/N 0102-014-6601 |

SECURITY CLASSIFICATION OF THIS PAGE (When Data Entered)

The concentration measurements of injected fluid in a turbulent water flow require a non-intrusive, high speed technique in order to capture the high frequency concentration fluctuations without disturbing the flow. A Laser-Induced Fluorescence (LIF) technique was evaluated where special attention was directed towards the theoretical background and its application in the laboratory. Concentration measurements were performed during the injection of dyed water and a dyed, aqueous solution of a polyacrylamide into a fully-developed turbulent channel flow.

A mass balance performed on a two-dimensional control volume using independent measurements of the streamwise velocity and the mean concentration yielded a significant deficit. Since it was unreasonable to attribute the imbalance to uncertainties in the measurements of the streamwise velocity, the main objective of this study was to carefully evaluate the concentration measurement technique. After having investigated the performance of the injector slot with respect to uniform injection, different experimental parameters that have an impact on the concentration measurements were varied. In the case of water-injected flow, it could be shown that the instantaneous array voltages have to be kept within a certain range which has to be determined prior to the experiment and depends on the saturation of the photo-diodes which are charged-coupled devices.

In the case of polymer-injected flow, the additional issues that influence the evaluation of the mass flux are nonuniform injection and a displacement of the probe volumes in the high concentration, near-wall region.

TABLE OF CONTENTS

Page

List of Symbols

Symbol	Description
α	fraction of available collected light
A_n	calibration constant for photodiode array element n
B	constant in law of the wall (equation 3.3)
C	instantaneous additive concentration
C_{inj}	injected concentration
C_{chan}	channel background concentration
D_{ab}	molecular mass diffusion coefficient
I_f	intensity of fluorescent emission
$I_e(y)$	intensity of excitation laser beam
I_o	initial intensity of excitation laser beam
P_{Las}	laser power
$\dot{Q}_{inj}$	injector flowrate based on linear sublayer ($y^+ \leq 8$)
$R_{\dot{Q}}$	mass flux ratio (equation 1.4)
$R_{\overline{uc}}$	correlation coefficient for streamwise mass transport, $R_{\overline{uc}} = \overline{uc}/u'c'$

T_s	array exposure time
U_i	instantaneous velocity components in index notation: U, V, W
U_m	mass-averaged velocity
U_o	center-line velocity
V_{dn}	dark-level voltage from photodiode array element n
V_n	output voltage from photodiode array element n
a	exponent relating photodiode voltage to fluorescence intensity (equation 2.6)
b_n	sensitivity of photodiode array element n
c	instantaneous concentration fluctuation, $c = C - \overline{C}$
d	y-direction length of concentration measurement volume
k	extinction coefficient for dye
n	number of photodiode
s	spacing of concentration measurement volumes
t	time
u_i	instantaneous velocity fluctuation components in index notation: $u = U - \overline{U}$, $v = V - \overline{V}$, $w = W - \overline{W}$
u_τ	shear velocity, $u_\tau = \sqrt{\tau_w/\rho}$

$u_i c$	instantaneous turbulent mass transport components in index notation
w	channel width
w_s	injector slot width
x_i	cartesian position vector in index notation: x, y, z
Ω	solid angle
α	fraction of available collected light
β	proportionality constant relating the dye extinction coefficient to the dye concentration
η	collection optics efficiency
κ	van Karman constant in law of the law (equation 3.3)
μ	dynamic viscosity
ν	kinematic viscosity
ρ	density
ϕ	quantum yield of dye molecule
τ_w	wall shear stress

Superscripts

$+$	normalized with inner variables u_τ and ν
$\bar{}$	time average

root mean square (RMS)

1. INTRODUCTION

The injection of soluble, long-chain polymer molecules into turbulent water flows has been known to cause drag-reduction through the modification of the structure of the turbulent boundary layer (see Tiederman, 1990 and Luchik and Tiederman, 1988). The modifications have been observed mostly in the buffer region by Tiederman (1990), Walker and Tiederman (1990), Luchik and Tiederman (1988), McComb and Rabie (1982), Willmarth et al. (1987) and others. With the exception of the study by Walker and Tiederman (1988), very little attention has been given to the near-field mixing region downstream of an angled, flush-mounted injector slot. In this study, polymer solutions at a concentration of 700 ppm (by weight) as well as plain water were injected into a fully developed turbulent channel flow to investigate further the initial mixing of the injector fluid. The mixing process is dominated by turbulent transport since the molecular Schmidt number for polymer diffusion is typically on the order of several hundred. The governing Reynolds-averaged equation for the conservation of a scalar quantity, C, in a stationary flow field can be written as follows:

$$\overline{U_i}\,\frac{\partial \overline{C}}{\partial x_i} = \frac{\partial}{\partial x_i}\left[D_{ab}\frac{\partial \overline{C}}{\partial x_i} - \overline{u_i c}\right] \tag{1.1}$$

Due to the time-averaging process, the new unknowns, $\overline{u_i c}$, are introduced. These represent the transport of species through fluctuations in concentration and velocity.

The suggested reduced form for the turbulent channel flow assuming the flow is on average two dimensional is

$$\bar{U}\frac{\partial \bar{C}}{\partial x}+\bar{V}\frac{\partial \bar{C}}{\partial y}=\frac{\partial}{\partial x}\left[D_{ab}\frac{\partial \bar{C}}{\partial x}-\overline{uc}\right]+\frac{\partial}{\partial y}\left[D_{ab}\frac{\partial \bar{C}}{\partial y}-\overline{vc}\right]. \qquad (1.2)$$

The additional unknowns in this equation must be related to the known quantities in the flow to enable calculation of the turbulent mixing process by introducing turbulent mass diffusivities. The usual thin-shear layer approximation yields an equation in which any changes in the streamwise direction on the right-hand side of equation (1.2) are neglected, i.e. $\frac{\partial(\,)}{\partial x}=0$. However, previous independent measurements of the streamwise velocity, $\bar{U}$, and the time-averaged concentration, $\bar{C}$, immediately downstream of the injector slot by Walker and Tiederman (1989) indicated that this assumption might be invalid in the initial mixing region. This problem became apparent because a mass balance performed on a two-dimensional control volume yielded a significant mass deficit. In fact, the mass flux calculated from the concentration and velocity measurements was up to four times larger than the injected mass flux. This mass balance is expressed as

$$\frac{\dot{Q}_{inj}\,C_{inj}}{w_s}=\int_0^{h/2}(\bar{U}\bar{C}+\overline{uc})\,dy \qquad (1.3)$$

where $\dot{Q}_{inj}$ is the injector flow rate, C_{inj} is the dye concentration of the injector fluid and w_s represents the width of the injector slot. This relation was developed based on the following assumptions:

1) turbulent, fully developed, channel flow which is homogeneous with respect to the spanwise direction;

2) uniform injection through the slot; and

3) steady flow.

It was unreasonable to attribute the mass imbalance to an uncertainty in the measurements of the streamwise velocity which was less than 0.5 per cent, according to Walker and Tiederman (1988). Therefore, the primary objective of this study was to determine the cause of the apparent mass balance deficit.

In the next chapter, the experimental apparatus and procedures for this study are presented and discussed. Extreme attention is given to the derivation of the working equation for the concentration measurement and the data acquisition procedure that allowed non-intrusive and high-speed measurements. The main emphasis of the third chapter is to present a number of measured concentration profiles that were obtained during the injection of dyed water. The mass flux terms in equation 1.3 will be calculated and presented for each case while the sensitivity of the concentration measurement technique on the mass flux ratio

$$R_{\dot{Q}} = w_s \frac{\int_0^{h/2} (\overline{U}\overline{C} + \overline{uc})\, dy}{\dot{Q}_{inj}\, C_{inj}} \tag{1.4}$$

will be investigated. In addition, some effects that are solely due to the presence of polymer solutions will be discussed.

2. EXPERIMENTAL APPARATUS AND PROCEDURES

2.1 Experimental Facilities

The recirculating water loop was driven by four 340 liters per minute centrifugal pumps yielding a maximum Reynolds number of about 40,000 based on the channel height. The test section had a rectangular cross-section (60 mm high and 575 mm wide) where the fluid was injected through flush-mounted, angled slots located in both the top and bottom walls about 80 channel heights downstream of the channel inlet. A schematic of the flow loop is shown in Figure 2.1. The width of the injector slots, measured in the streamwise direction, was 2.5 mm and they were inclined at an angle of 25 degrees relative to the mean flow direction as shown in Figure 2.2. The slot dimension in the spanwise direction, w_s, was 475 mm. The coordinate system used in this experiment and its orientation with respect to the mean flow axis is shown in the same Figure. The origin of the coordinate system is located at the center (mid-span) of the bottom injector slot. A more detailed description of the flow facilities can be found in Walker and Tiederman (1990).

2.2 The Laser-Induced Fluorescence (LIF) Technique

Time-resolved concentration measurements were obtained using a laser-induced fluorescence (LIF) technique similar to the one employed by Koochesfahani and Dimotakis (1986). The injected fluid was marked with a fluorescent dye which has a time scale for molecular diffusion that is three orders of magnitude larger than the time scale associated with turbulent dispersion. The dye used in this experiment was

fluorescein disodium salt and the solution was excited by a laser beam directed normal to the channel wall (y-direction). The spatial distribution of the intensity of the fluoresced light was measured using a Reticon line-scan camera that incorporated a line array of 256 photodiodes. The photodiodes are 25 μm by 425 μm and located on 50 μm centers. The magnification used in the experiment was varied and yielded effective measurement volumes that were spaced between 56.3 μm and 95.2 μm in the direction normal to the wall.

The blue line (488 nm) of a Lexel model 85.5 argon-ion laser was used to excite the dye. Focusing the beam with a 200 mm focal length lens yielded a beam diameter of 115 μm across the field of view and hence determined the spatial resolution of the measurement volume. Please note that an optical filter was *not* used to eliminate 488 nm scattered light from the light imaged on the photodiodes. Since the water had been filtered and dearated, it was assumed that the small amount of Rayleigh scattering could be eliminated from the results by subtraction of a background reading that will be discussed in Section 2.2.2.

The dye concentration at a point along the beam path was determined from the intensity of the fluorescent emission. Finally, the injectant concentration was inferred from the measured dye concentration.

2.2.1 Theoretical Background of the LIF Technique

The laser-induced fluorescence technique provides a powerful tool in measuring concentration profiles without disturbing the flow. This non-intrusive technique is

based upon the characteristic of a fluorescent dye to be an appropriate, high molecular Schmidt number marker. The following analysis shall provide the physical background that describes the LIF technique and present working equations and their applications in the laboratory where special attention will be directed towards the experimental procedure and to all parameters that have to be controlled carefully in order to obtain an accurate measurement.

For the derivation of the working equation, the following assumptions were made:

1) no saturation of excited dye molecules;

2) negligible attenuation of fluorescent light along the receiving path; and

3) no preferable polarization direction of the fluorescent light.

Starting with the general expression for light propagating in an absorbing medium and integrating yields the intensity of the laser beam to excite the dye, I_e

$$I_e(y) = I_o e^{-\int_0^y k(r)dr} . \qquad (2.1)$$

where $I_o=I_e(y=0)$ and k is the extinction coefficient which is assumed to be proportional to the dye concentration, C, for the concentrations of interest. Therefore, $k = \beta C$. It should be noted that the proportionality constant β depends strongly on the pH of the liquid unless the pH exceeds 8.0. The fluorescent light intensity is some fraction of the light absorbed over a small segment of length d according to

$$I_f(y) = \alpha\phi\beta C I_e(y) d \qquad (2.2)$$

where α is some fraction of the available collected light and is related to the f-number

of the camera lens and ϕ is the quantum yield of the dye molecule. Combining the above equations yields

$$I_f(y) = \alpha\phi\beta C(y) I_o e^{-\int_0^y \beta C(r)dr} d . \tag{2.3}$$

Solving for the local concentration C(y) and accounting for a constant concentration over a small segment, s, the integration can be replaced by a summation and the average dye concentration C_n at the n^{th} segment of the excitation laser beam is given by

$$C_n = C(y_n) = \frac{I_{fn}}{I_o \alpha\phi\beta d} e^{\sum_{i=1}^{i=n-1} \beta C_i s} \tag{2.4}$$

which can be rewritten as

$$C_n = \frac{1}{I_o \alpha\phi\beta d} \left[\prod_{i=1}^{i=n-1} e^{\beta C_i s} \right] I_{fn} . \tag{2.5}$$

The intensity I_{fn} is related to the voltage at the n^{th} element of the photodiode array by

$$\eta \frac{\Omega_n}{4\pi} T_s b_n I_{fn} = (V_n - V_{dn})^{a} , \tag{2.6}$$

where η is the collection optics efficiency which accounts for losses due to reflection and absorption, Ω_n is the solid angle as viewed by the n^{th} element, T_s is the exposure time, b_n the sensitivity of the n^{th} photodiode and V_n and V_{dn} the voltage and dark-level voltage of the array, respectively. The charged-coupled device has a first order response such that the relationship between the fluorescence intensity and the photo-diode array voltage is non-linear. The exponent, $a = 0.837$, was determined by a calibration procedure. Combining equations 2.6 and 2.5 yields

$$C_n = \left[\frac{1}{I_o \alpha \phi \beta d \eta \frac{\Omega_n}{4\pi} T_s b_n}\right] \left[\prod_{i=1}^{i=n-1} e^{\beta C_i s}\right] (V_n - V_{dn})^a . \qquad (2.7)$$

This equation relates the dye concentration at the n^{th} element to the measured voltage.

For simplicity, we introduce the element constant

$$A_n = I_o \alpha \phi \eta \frac{\Omega_n}{4\pi} b_n T_s \beta d = a_n I_o T_s , \qquad (2.8a)$$

with

$$a_n = \alpha \phi \eta \frac{\Omega_n}{4\pi} b_n \beta d = \frac{A_n}{I_o T_s} , \qquad (2.8b)$$

which has to be determined prior to each injection experiment. The calibration factor has been rewritten as shown in equation 2.8b to allow for a variable laser power (changing I_o) and a variable exposure time (changing T_s). Finally, we are able to rewrite equation 2.7 using the previous expressions for the element calibration constant a_n

$$C_n = \frac{1}{a_n I_o T_s} \left[\prod_{i=1}^{i=n-1} e^{\beta C_i s}\right] (V_n - V_{dn})^a . \qquad (2.9)$$

2.2.2 Application of the LIF Technique

It is necessary and absolutely crucial to fully understand all physical relations that are involved in this technique to correctly apply it in the laboratory. The appropriate choice of the marker fluid and the excitation laser wavelength has to account for

separate peaks in the spectrums for the excitation and the fluorescence. In this experiment, this has been accomplished by chosing the blue line ($\lambda_e = 488$nm) of a 500 mW Argon-ion laser to excite an aqueous solution of fluorescein disodium salt whose fluorescent spectral peak occurs at $\lambda_f = 518$nm.

Prior to each injection experiment, the constant for each element of the photodiode array has to be determined. The calibration factors, a_n, for the photodiode array are calculated by placing a known uniformly distributed dye concentration into the channel and measuring the voltages on the array. Rearranging equation 2.9 with $C_n = C_{chan} = \text{const.}$ yields

$$\overline{(a_n I_o)}_{off} = \frac{\exp[(n-1)\beta C_{chan} s]\ \overline{(V_{n,off} - V_{dn})}^{\,a}}{T_{s,off} C_{chan}} \tag{2.10}$$

where C_{chan} is the constant background concentration in the channel, and $V_{n,off}$ is the measured offset voltage. This calibration procedure requires that the product $\overline{(a_n I_o)}_{off}$ remains constant during the course of the experiment.

During the injection experiment, the sum of the background and injector concentration is measured for each individual scan (index k). A correction factor is introduced which accounts for small instantaneous changes in the excitation laser power. The laser power is constantly monitored and stored for each scan, so that equation 2.9 gives the following relationship between the measured voltages and the instantaneous local additive concentration,

$$C_{nk,tot} = C_{nk} + C_{chan} = \frac{1}{\overline{(a_n I_o)}_{off} T_{s,inj}} \left[\prod_{i=1}^{i=n-1} e^{\beta C_{ik,tot} s} \right] (V_{nk} - V_{dn})^a \left[\frac{\overline{V_{L,off}}}{V_{Lk}} \right] \quad (2.11)$$

Solving equation 2.11 for the injectant concentration C_{nk}, the final form of the working equation is

$$C_{nk} = \frac{1}{\overline{(a_n I_o)}_{off} T_{s,inj}} \left[\prod_{i=1}^{i=n-1} \exp(\beta C_{ik,tot} s) (V_{nk} - V_{dn})^a \left[\frac{\overline{V_{L,off}}}{V_{Lk}} \right] \right] - C_{chan} \quad .(2.12)$$

2.3 The Laser-Doppler Velocimeter (LDV)

In addition to the LIF-technique, a single-component dual-scatter laser velocimeter was used to measure the streamwise (x-direction) velocity component. For this purpose, a Spectra-Physics Inc. model 106-1 10 mW HeNe laser in conjunction with the TSI model 9100-8 transmitting system was used. After passing a TSI model 9115-1 beam splitter, the polarization of the beam was rotated using a quarter-wave plate. One beam was frequency shifted by 40 MHz with a TSI model 9182-12 Bragg cell to eliminate fringe bias. The beams spaced by 50 mm passed through a 2.27 beam expander before they were focused using a 250 mm transmitting lens. The optical arrangement for both optical measurement techniques is shown in Figure 2.3.

Locating the axis of the receiving optics at an angle of 9.5 degrees to the plane given by y=const yielded an effective length of the probe volume (in the spanwise direction) of l_z=1291μm, or in terms of the dimensionless wall coordinate, l_{z^+}=37.1. The extent of the probe volume in the y-direction was l_y=107μm which corresponded to l_{y^+}=3.1. The receiving optics incorporated a 250 mm focal length lens, a 2.27 telescope

and one photomultiplier tube including a narrow band-pass optical filter centered at 632.8 nm.

An electronic downmixer yielded an effective frequency shift of 0.5 MHz. The downmixed signal was high-limit and low-limit filtered at 1 MHz and 300 kHz, respectively. The signal frequency was measured with a TSI model 1980 counter processor operating in the N-cycle mode. Adjusting the amplifier gain so that a maximum signal amplitude of 500 mV could be obtained, the signal-to-noise ratio was as high as 50:1. Finally, a TSI model 1988 digital to analog converter generated an analog velocity trace when the validation requirements were met. The flow was seeded with the fat particles from homogenized whipping cream. To eliminate velocity bias, the analog velocity signal was sampled at equal time intervals and the velocity statistics were calculated from ensembles of 10,000 data realizations.

2.4 Experimental Procedures

The exposure time for the concentration measurements was typically 333 μs when water was injected and 500 μs for polymer injected flows. However, the exposure time was varied in some cases where water was injected to determine its influence on the measurements results. All data were acquired at a rate of 200 Hz by digitizing either every fifteenth concentration scan (water) or every tenth scan (polymer) and ensembles of 10,000 data points were used to calculate the statistics. One data record took 50 seconds which corresponded to approximately 250 burst events in the case of a Newtonian channel flow.

When aligning the line-scan camera with the excitation beam, it was crucial to locate the photodiode array relative to the wall because the first diode at the wall determined the initial intensity I_o which is a term in the calculation of the concentration profiles. For this purpose, the integration time on the camera was increased and the probe volume of the HeNe LDV was focused on the array. The position of the measurement volumes relative to the wall was established by determining the camera element number for two known positions in the flow field.

Three separate measurements were required for each data set. First, the dark voltage was determined by digitizing 1000 scans of the array with the excitation beam blocked. Simultaneously, the dark voltage of a separate photodiode that monitored the fluctuation in the laser light intensity was stored and calculated. Next, the background intensity in the channel was measured and the dye concentration of the water in the flow loop was determined using an attenuation cell. This cell allowed the determination of the concentration of a fluid passing through a cavity of known length by measuring the attenuation of a laser beam passing through the cell using a Lexel model 504 laser power meter. The dye concentration of the injector fluid was deduced from the known total volume of the mixture and the known dye concentration of the initial 5000 ppm (dye by weight) batch. Finally, the fluorescence intensity during an injection was measured with the photodiode array.

For simultaneous measurement of the streamwise velocity and additive concentration, spatial as well as temporal coincidence had to be guaranteed. Spatial coincidence was achieved by using the TSI model 9140 receiving assembly with an

eyepiece and by focusing the LDV probe volume on the eyepiece reticule and aligning it with the reticule cross-hairs. The excitation beam was aligned so that it stayed sharply focused and centered on the cross-hairs throughout the vertical traverse of the transmitting optics. In order to ensure temporal coincidence, the velocity signal was transferred to an additional channel of the A/D converter and sampled for each intensity profile digitized. A block diagram of the electronics is shown in Figure 2.4.

2.5 Preparation of Polymer Solution

For the drag-reducing injection experiments, an aqueous solution of SEPARAN AP-273, a polyacrylamide manufactured by Dow Chemical, at a concentration of 700 ppm (based on weight) was used. The polymer solution was prepared following a standard procedure to ensure repeatability of thermophysical properties. First, the required amount of dry powder was suspended with isopropyl alcohol and then mixed with filtered, deaerated, softened tap water at about 38°C using a magnetic stirrer. This solution was allowed to hydrate for 12 to 24 hours. The initial concentration of approximately 5000 ppm was then diluted to the desired concentration with filtered, softened tap water.

An investigation by Walker (1987) showed that the fluorescence of the dye is very sensitive to pH variations near the neutral value. In both cases (water and polymer injections), the pH of the channel water and the injectant fluid were matched at a value of 8.8 (for water) and 8.1 (for polymer) respectively to eliminate uncertainties of the concentration measurements due to changes in pH.

Prior to the experiment, two different methods for mixing the dye and the polymer were investigated in a separate bench test to determine the response of fluorescence intensity on dye concentration in the polymer solution and the mixing procedure. In the first case, dye was added to the polymer solution immediately before the test was conducted and the voltage of a specific photodiode of the camera array was measured for different dye concentrations in the range of interest. For the other method which was initially applied by Brungart and Petrie (1990), the required amount of dye was added to the filtered tap water before the 5000 ppm solution was diluted to its final concentration so that the polymer could hydrate with the dyed water. In both cases, the fluorescence intensity was proportional to the dye concentration which indicated that the response of the dye molecule, when mixed with a polymer solution, was independent of the mixing procedure. A more detailed description of the experimental apparatus and procedure including the results of this test can be found in the appendix. In this experiment, the latter method was chosen to dye the injectant fluid.

3. RESULTS

One-component LDV measurements of the streamwise velocity without injection were initially made to establish flow conditions and to verify the nature of the Newtonian flow. These data were also used as a reference to the measurements made during injections. The mass-average velocity which was maintained constant during the course of all the experiments at 0.578 m/s which yielded a Reynolds number (based on the channel height) of 36100 and a shear velocity, u_τ, of 0.0277 m/s in the fully

developed channel flow of water. The fluids were injected through both the top and bottom slot at the linear sublayer flow rate (1.0 l/min through each slot) based on a sublayer thickness of $y^+ = 8$ for the undisturbed flow. When data are presented in normalized inner coordinates, the shear velocity for the undisturbed case and the solvent viscosity are used. Prior to each set of injection experiments, flow visualization was used to determine the slot performance for both water and polymer injected flows.

3.1 Water Injection

In the case of the injection of a dyed water solution, the uniformity of the injection was tested using the blue line (488 nm) of the Argon-Ion Laser and aligning it in the spanwise direction (z-axis) and very close to the slot ($x \simeq 10$mm). Dyed water was injected and it could be clearly seen that the fluorescent region from the dyed fluid was uniformly thick across the entire slot width indicating that the injection was uniform throughout the slot during water injection.

The measurement of concentration profiles of dyed water into a turbulent, fully-developed channel flow using the laser-induced fluorescence technique described in the previous chapter involves less complications than the accurate determination of concentration profiles downstream of an additive injector when polymer solutions were injected. In this section, the difficulties associated in measuring water concentrations are discussed first before additional difficulties present during polymer injection are discussed.

The influence of certain parameters on the mass balance of the injector fluid on a two-dimensional control volume will be characterized by the mass flux ratio as defined in equation 1.4 and rewritten in the following way

$$R_{\dot{Q}} = \frac{\dot{Q}_{out}}{\dot{Q}_{in}} = \frac{w_s}{\dot{Q}_{inj} C_{inj}} \int_0^{h/2} (\overline{U}\overline{C} - R_{\overline{uc}} u'c') \, dy \,, \qquad (3.1)$$

where the correlation coefficient, $R_{\overline{uc}}$, was assumed to be equal to 0.5. This assumption allowed us to use non-simultaneous concentration data to evaluate how variations in the concentration measurement technique affected the mass balance. As will be shown later a value of 0.5 is close to the maximum measured from the one set of simultaneous velocity and concentration data. The integral was evaluated numerically using the trapezoidal rule.

The significance of the non-linear relationship between the fluorescence intensity I_{fn} and the photo-diode element voltage, V_n is shown in Figure 3.1. There is a significant but not complete reduction in the mass balance deficit when the non-linear relationship is used compared to assuming that the relation between the fluorescence intensity and the array voltage is linear, i.e. the exponent in equation 2.6 becomes a = 1.

In Figure 3.2, the additive concentration is plotted for different locations downstream of the injector slot. The significant decrease of mass flux ratio with increasing x-location suggests there was a problem associated with the presence of a thin, high concentration layer near the slot. This observation indicates that there may be a problem associated with the spatial resolution of thin, high concentration fluid layers.

In order to enhance the resolution of the high concentration layer, two parameters were changed. Concentration profiles were measured for water-injected flows at x=25 mm downstream of the injector slot varying the injector flow rate in one case and the magnification factor of the optics in the other case. In Figure 3.3, the mean concentration profiles for different injector flow rates, varying between 1 l/min and 5.3 l/min, show that an increasing flow rate results in an extension of the high concentration region near the wall and an increase in the wall concentration at the same time. The mean concentration profiles for different magnification factors are shown in Figure 3.4, where the injector flow rate was 1 l/min in every case. The center to center spacing of the photodiode array in the field of view, s, was varied by changing the object and image distances of the optical system. It is apparent from this figure that the near-wall concentration decreased with increasing magnification factor which corresponds to a decreasing photodiode spacing, s.

In order to interpretate the effects of the varied parameters on the mass balance, the mass flux ratio, $R_{\dot{Q}}$, defined in equation 3.1, has been calculated for every concentration profile using available velocity data, and plotted as a function of the normalized photodiode spacing, $\frac{s}{\lambda}$, where λ is the wall-normal location where $\overline{C} = \frac{\overline{C}_{wall}}{2}$. The results of this analysis are shown in Figure 3.5. It includes one measurement made in a zero pressure gradient boundary layer during the injection of a 1000 ppm polymer solution by Koskie and Tiederman (1991). A clear trend can be seen for the calculations involving the variable magnification factor, demonstrating that the spatial resolution of the near-wall, high concentration layer measurement volumes improves

the mass balance factor $R_{\dot{Q}}$ which should be approximately 1.0. Initially, it was believed that the higher resolution for increasing magnification factors resulted in a more accurate evaluation of the attenuation term. However, subsequent calculations showed that an exclusion of the attenuation term, $\prod_{i=1}^{i=n-1} \exp(\beta C_i s)$, did not have a significant effect on the concentration profiles as shown in Figure 3.6.

In the case of a variable injector flow rate the data were fairly scattered. At the same time, the data indicated that the mass flux ratio improved even though the measurement volume resolution remained unchanged. This observation supports the previous result because it showed that the mass flux integral is highly sensitive to the resolution of the near-wall concentration layer.

The previous observations that were made with respect to the variation of the magnification factor indicated that the difficulties might be associated with the fact that the array voltages during the injection experiment may rise into the range where the diodes are close to their saturation level. This is outside the range over which the diodes are calibrated and would lead to an overestimate of the local concentration. In Figure 3.7, different concentration profiles are shown together with a table, listing the relevant experimental parameters as well as the average array voltage and the mass flux ratio, to demonstrate the impact of the average diode voltages on the measured concentration profile and the evaluated mass balance. In order to make the effect of the array voltage on the mass balance clearer, Figure 3.8 shows the mass flux ratio as a function of the average pixel voltage for the individual runs shown in Figures 3.7 and 3.4. This Figure clearly demonstrates the significant influence of the magnitude of the

voltages on the mass flux ratio. The average array voltage, $\overline{V}$, is a measure but it is the instantaneous voltage that matters with regard to accounting for pixel voltages that are out of range. It is reasonable to assume that the instantaneous voltages are

$$V \approx \overline{V} \pm 3v' \tag{3.2}$$

where v' is the standard deviation which is highest near the injector slot. This observation corresponds well with previous remarks made concerning the improvement in the mass balance further downstream of the injector slot.

An error analysis of the working equation for the LIF technique was performed to estimate the effect of experimental uncertainties. The inherent error sources for the concentration measurement procedure originate from uncertainties in determining the extinction coefficient, $\beta(\pm 4.0\%)$, the channel background concentration, $C_{chan}(\pm 7\%)$, and the dye concentration of the injector fluid, $C_{inj}(\pm 6\%)$. These are the estimated 95% confidence limits for these variables. Uncertainties due to changes in pH and temperature differences between the channel and injector fluid were assumed to be negligible, because both the channel water and the injectant were buffered with sodium hydroxide (pH > 8) and maintained at approximately the same temperature ($\Delta t \approx 0.2°C$). The error bound for the concentration was calculated and showed that the uncertainty in the concentration can not be neglected with respect to its influence on the mass flux ratio as seen in Figure 3.9. On the other hand, the uncertainty itself does not account fully for the mass balance discrepancies near the slot.

In another test, concentration profiles were measured using different integration times. When evaluating the statistic quantities of a turbulent flow using experimental

data, one has to make sure that the duration of the data record will account for all the structures that are present in the turbulent flow field. The appropriate integration time has to be significantly larger than the largest expected time scale in the flow. In order to address this issue, concentration data were taken for two different integration times. As shown in Figure 3.10, a change in the integration time does not effect the mass flux ratio since the difference in concentration values are within the error bounds. This observation indicates that the shorter integration time (T = 20 sec) is sufficient in this flow field.

During the course of the experiment, it became obvious that the channel walls had to be absolutely clean. Scattered light due to dirt particles on the wall where the excitation beam entered the flow channel, caused the calibration factor array, A_n, to be overpredicted resulting in the calculation of low, near-wall concentration values. This problem was eliminated by cleaning the channel wall prior to the experiment.

In Figure 3.11, the normalized mean streamwise velocity for Newtonian flows with water injection is compared with the flow where no fluid had been injected. For the case without injection, the different regions (linear sublayer, buffer and log-law region) could clearly be distinguished. The solid line in the log-law region is represented by

$$U^+ = \frac{1}{\kappa} \ln y^+ + B \tag{3.3}$$

and the relationship for the near-wall variation (linear sublayer)

$$U^+ = y^+ \tag{3.4}$$

The agreement between the lines and the data for the water flow without injection and

there is good correspondence with the logarithmic law using the values $\kappa = 0.41$ and $B = 6.0$ which were recommended by Luchik and Tiederman, 1987.

The near-wall velocities ($y^+ < 30$) for the two locations nearest to the injector slot are clearly lower than the other data when water is injected. In order to satisfy continuity the flow in the outer region is accelerated. The extent of the near-wall region of the decelerated flow corresponds to the high concentration layer of the injector fluid (see Figure 3.3). Further downstream of the injector slot, the velocity profile with water injection corresponds better to the standard channel flow profile.

Figure 3.12 shows the root-mean-square (RMS) velocity fluctuation in the streamwise direction under the same conditions as in the previous figure. In every case the peak in $\frac{u'}{u_\tau}$ occurs at about the same location ($y^+ = 15$) and reaches a maximum value of approximately 3.0 except for the location nearest to the slot ($x = 10$ mm) with water injection where it reaches 3.4. There is good agreement for the rest of the data with that of Walker and Tiederman (1990) and Kreplin and Eckelmann (1979).

Finally, simultaneous measurements of the instantaneous velocity and concentration product are presented in Figure 3.13 to show how the streamwise turbulent mass transport varies downstream of an additive injector when dyed water is injected into a fully turbulent channel flow. Here, the time-averaged product of the streamwise velocity and concentration fluctuation, $\overline{uc}$ normalized with the injectant concentration and the shear velocity as a function of y^+ is shown. Although there is high scatter in the data near the injector slot, the turbulent streamwise mass transport decreases steadily with downstream distance inside the high concentration layer. Beyond $y^+ = 100$, values

of $\overline{uc}$ for x = 50 mm and 100 mm are larger than the values for the locations nearer to the slot. This increase shows that the turbulent mixing activity further away from the wall increases as the fluid convects downstream. At a location 25 mm downstreeam of the injector slot and 1 mm from the wall $\frac{\partial}{\partial x}\overline{(uc)}$ was about 4 % of $\frac{\partial}{\partial y}\overline{(vc)}$. This indicates that the streamwise derivative of the turbulent streamwise mass transport, $\frac{\partial}{\partial x}\overline{(uc)}$, is not significant for Newtonian flows with water injection.

The correlation coefficient for turbulent streamwise mass transport $R_{\overline{uc}} = \frac{\overline{uc}}{u'c'}$ is shown in Figure 3.14. For the channel flow with water injection there is significant scatter that reflects the scatter in $\overline{uc}$. Notice that the correlation coefficient increases with increasing distance from the injector slot. This indicates that the fluctuations contribute more to the net mass transport as the fluid moves downstream. A peak value of approximately 0.6 occurred at about a y^+ of 70 at x = 100 mm.

3.2 Polymer Injections

Despite the effects on the mass balance deficit mentioned in the previous section, there are additional issues that require close attention when polymer is injected into the flow. In polymer-injected flows, a flow visualization experiment was conducted to investigate the performance of the injector slot with drag-reducing additives. At a downstream location of x = 100 mm, a laser light sheet oriented parallel to the bottom wall at $y^+ \simeq 20$ was created using a combination of a spherical focusing lens and a cylindrical lens. Two, three-minute records were taken using a standard video camera

operating at 30 frames per second and the streak structure was analyzed by seven independent observers. The screen was divided into several bins whose width was on the same order as the streak spacing. Each observer analyzed 20 statistically independent frames that were separated by 10 seconds. A streak was identified when a distinct high concentration filament that had a streamwise length of at least four times the estimated streak spacing. The average number of streaks for each bin was calculated from the total number of events for each bin divided by the number of frames and the number of independent observers. The results of this investigation are shown in Figure 3.15 and it can be clearly seen, that the streaks were not uniformly distributed with respect to the spanwise direction. It is apparent that there is a lower flow rate of injected fluid in the spanwise center span of the injector. This should result in a value for the injected mass flux that is less than one.

During the injection of polymer solutions, it became apparent that the measurement volumes in the near-wall, high concentration region were displaced due to a change of indices of refraction. An experiment was set up to quantify the probe volume displacement by focusing the LDV probe volume onto the camera array and measuring the photo element voltages with and without injection of a 700 ppm polymer solution.

Figures 31.6 through 3.20 show the average array voltages for a number of different cases where the axial location (x-axis) and the location normal to the wall (y-axis) were changed. The data were taken during the injection of an undyed and a dyed (2 ppm of fluorescein dye) aqueous solution of polyacrylamide. The perpendicular lines in the plots indicate the amount by which the probe volume was shifted on average towards

the wall due to a higher index of refraction of the near-wall high concentration layer. In Figure 3.16, the array voltages are shown for the probe volume located at x = 25 mm downstream of the injector slot and y = 1.0 mm which corresponds to $y^+ \approx 30$. In this case, the probe volume was shifted by four viscous units due to the presence of the polymer. Further downstream of the slot at x = 100 mm, the average shift is about five viscous units (Figure 3.17) at the same y location (y = 1.0 mm). As shown in Figure 3.18, the shift becomes negligible at y = 1.5 mm. It has to be noted that the first peak closest to the wall in the array voltage distribution for polymer injected flows is due to a reflection of the probe volume by the bottom wall. Finally, the previous two locations were repeated where dyed polymer was injected instead of undyed fluid. The results are shown in Figures 3.19 and 3.20 and they clearly show that the dyed fluid causes a larger shift of the probe volume; six and a half viscous units in Figure 3.19 and three units in Figure 3.20. This behavior addresses an additional problem when accurate concentration measurements of polymer solutions are desired.

4. CONCLUSIONS AND RECOMMENDATIONS

The difficulties associated with the LIF technique that has been used to measure concentration profiles of water and polymer injection into a turbulent, fully-developed channel flow have become apparent. The LIF technique was described in detail and several hypothesis were tested with respect to their impact on a mass balance performed on a two-dimensional control volume. It could be shown that the measurements were very sensitive to the magnification factor of the imaging system and that the mass balance deficit decreased as the downstream distance increased. These difficulties indicate that the main problem in evaluating the mass flux integral (right-hand side of equation 1.3) is due to the voltage level on the photo-diode array. It became obvious that the average voltage level on the photodiode array had to be kept fairly low in order to keep the instantaneous voltage levels within the calibrated range.

It remains to be determined whether this technique is sensitive enough to make an accurate evaluation of the mass flux integral in the near field of an injector. It is necessary to keep the voltage levels within the range for which the photo-diode array was calibrated. Therefore, the magnification factor, the excitation laser intensity and the array exposure time have to be selected such that the instantaneous array voltages are within the desired range.

In order to meet this goal, a number of concentration profiles were taken where the exposure time was different during the experiment than the time used during the calibration procedure which is necessary to determine the calibration factors of the

array. However, the results that are documented in a second appendix indicate that this procedure requires further investigation due to a constant offset of the concentrations far away from the wall.

REFERENCES

Brungart, T.A. and H.L. Petrie 1990 A laser-induced fluorescence technique for measurement of slot-injected fluid concentration profiles in a flat plate turbulent boundary layer. *Technical Report No.* **TR 90-006** , Penn State University.

Koochesfahani, M.M. and D.E. Dimotakis 1986 Mixing and chemical reactions in a turbulent mixing layer. *J. Fluid Mech.,* **170** , 83.

Koskie, J.E and W.G. Tiederman 1991 Turbulence structure and polymer drag reduction in adverse pressure gradient boundary layers. *Report* **PME-FM-91-3** , Purdue University.

Kreplin, H. and H. Eckelman 1979 Behavior of the three fluctuating velocity components in the wall region of a turbulent channel flow. *Phys. Fluids,* **22** , 1233.

Luchik, T.S. and W.G. Tiederman 1988 Turbulent structure in low concentration drag-reducing flows. *J. Fluid Mech.,* **190** , 241.

Luchik, T.S. and W.G. Tiederman 1987 Timescale and structure of ejections and bursts in turbulent channel flows. *J. Fluid Mech.,* **174** , 529.

McComb, W.D. and L.H. Rabie 1982 Local drag reduction due to injection of polymer solutions into turbulent flow in a pipe. Part I: Dependence on local polymer concentration; Part II: Laser-Doppler measurements of turbulent structure. *AICHE J.,* **28** , 547.

Tiederman, W. G. 1990 The effect of dilute polymer solutions on viscous drag and turbulence structure. In: *Structure of Turbulence and Drag Reduction* , A. Gyr, ed., Springer Verlag, 187.

Walker, D.A. 1987 A fluorescence technique for measurement of concentration in mixing liquids. *J. Phys. E. Sci. Instrum.,* **20** , 217.

Walker, D.T. and W.G. Tiederman 1990 Turbulent structure in a channel flow with polymer injection at the wall. *J. Fluid Mech.,* **218** , 377.

Walker, D.T. and W.G. Tiederman 1989 The concentration field in a turbulent channel flow with polymer injection at the wall. *Exp. Fluids,* **8** , 86.

Walker, D.T. and W.G. Tiederman 1988 Turbulent structure and mass transport in a channel flow with polymer injection, *Report* **PME-FM-88-2** , Purdue University.

Willmarth, W.W, T. Wei, and C.O. Lee 1987 Laser anemometer measurements of Reynolds stress in a turbulent channel flow with drag-reducing polymer additives. *Phys. Fluids,* **30** , 933.

FIGURES

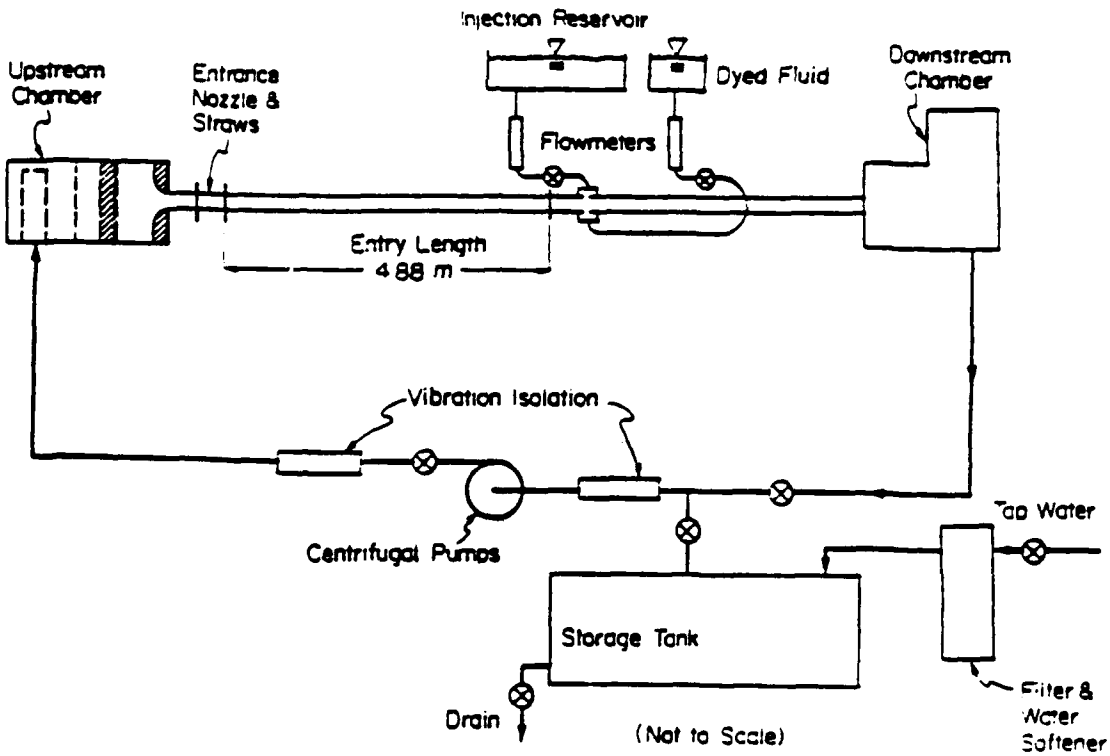

Figure 2.1: Schematic of flow loop (D.T. Walker and W.G. Tiederman, 1988).

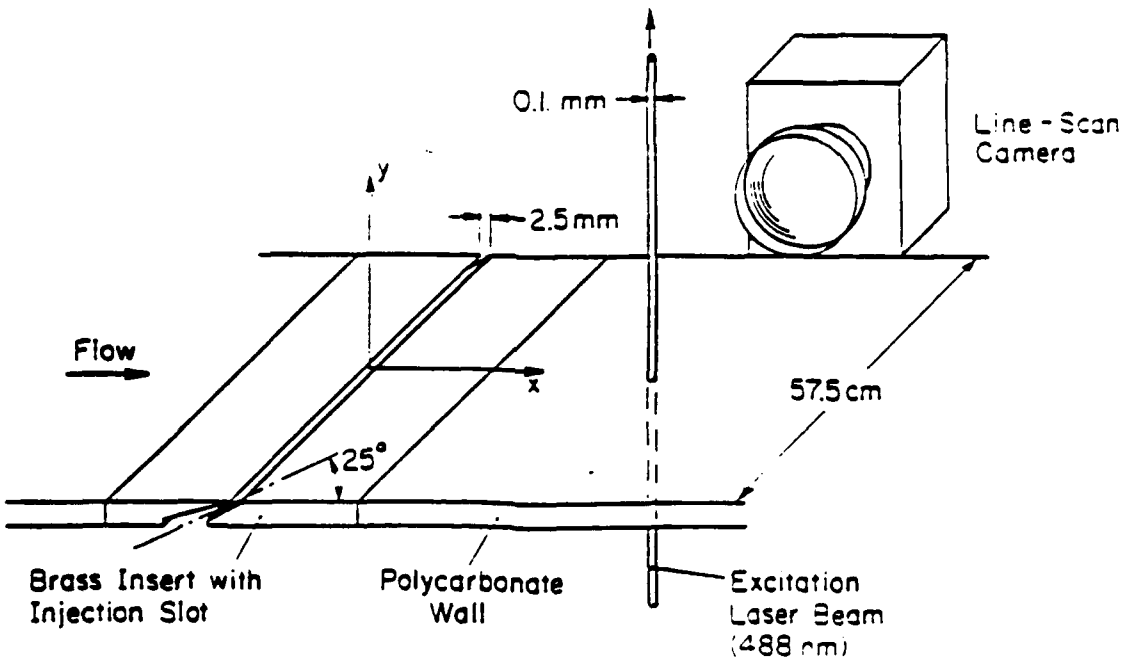

Figure 2.2: Injection slot and optical arrangement (D.T. Walker and W.G. Tiederman, 1988).

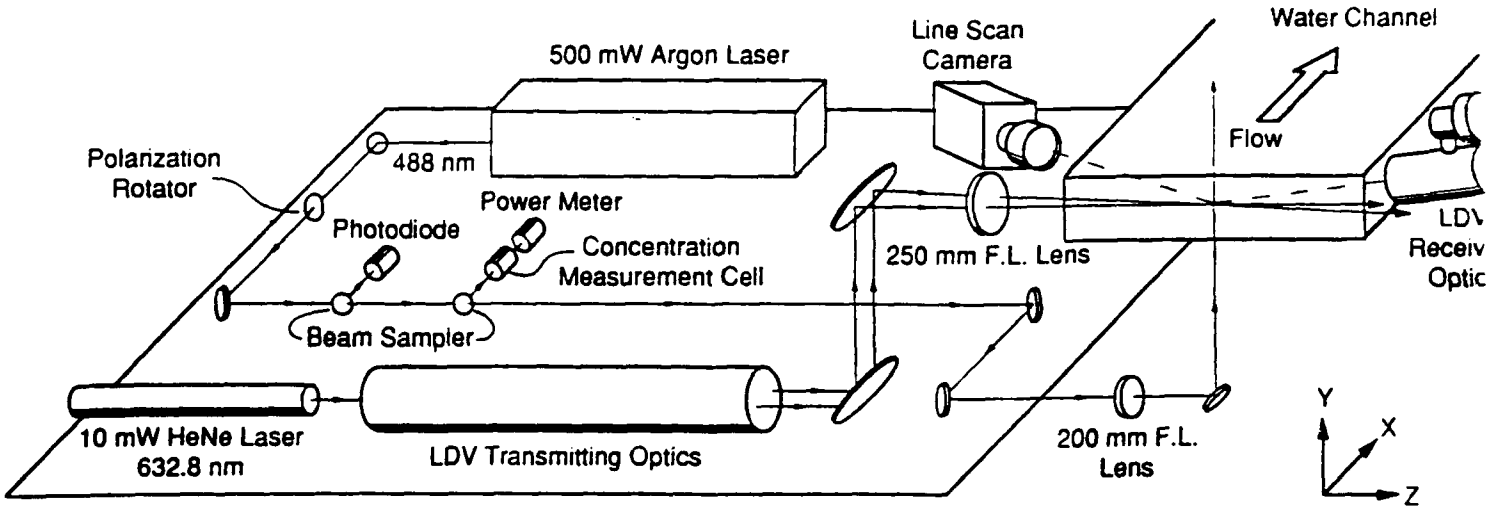

Figure 2.3: Schematic for velocity and concentration measurements (D.T. Walker and W.G. Tiederman, 1988).

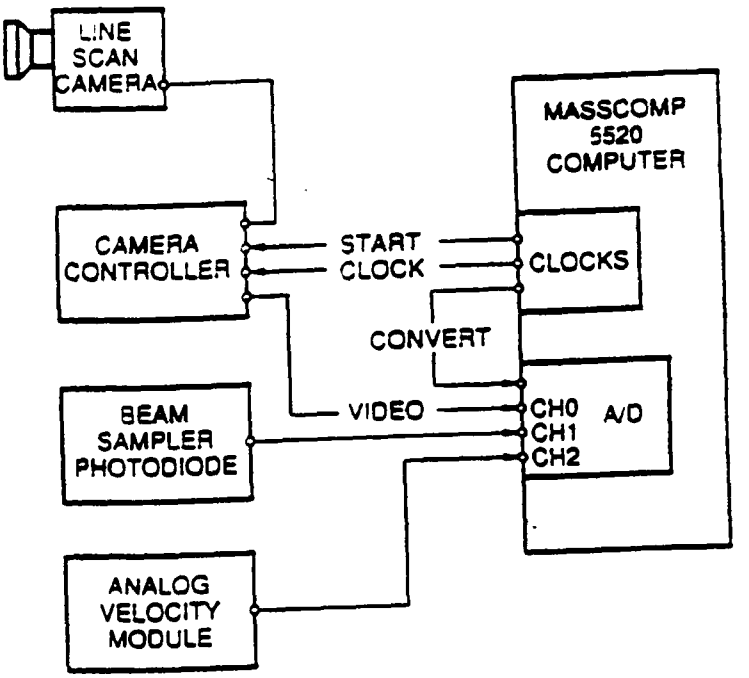

Figure 2.4: Block diagram of electronics for velocity and concentration measurement (D.T. Walker and W.G. Tiederman, 1988).

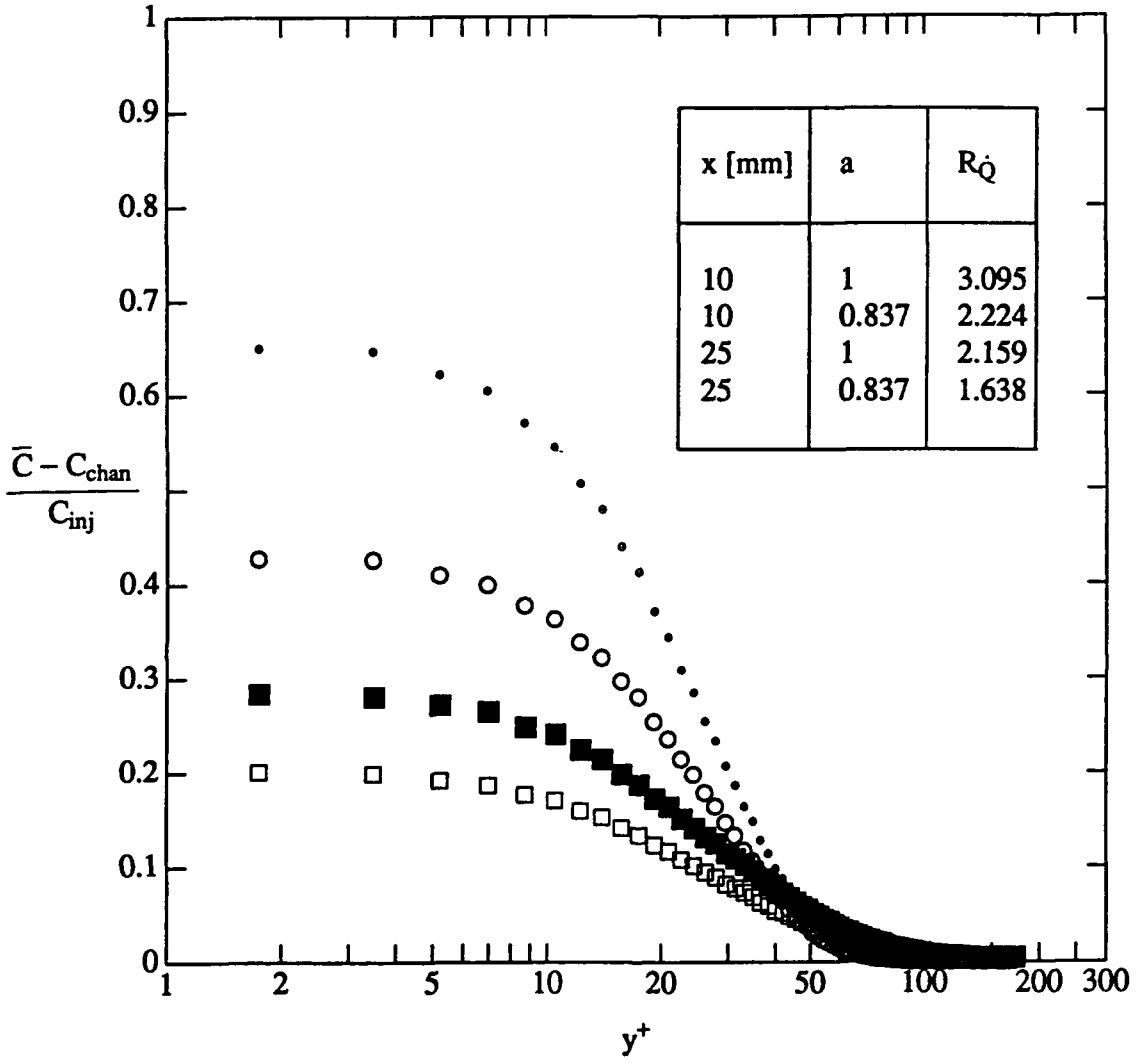

Figure 3.1: Inner normalized plot of mean concentration for water-injected flow using a linear and a nonlinear relation between the fluorescence intensity and the array voltage according to $I_f \propto V^a$; ○ - x=10 mm (a=0.837); • - x=10 mm (a=1.0); □ - x=25 mm (a=0.837); ■ - x=25 mm (a=1.0).

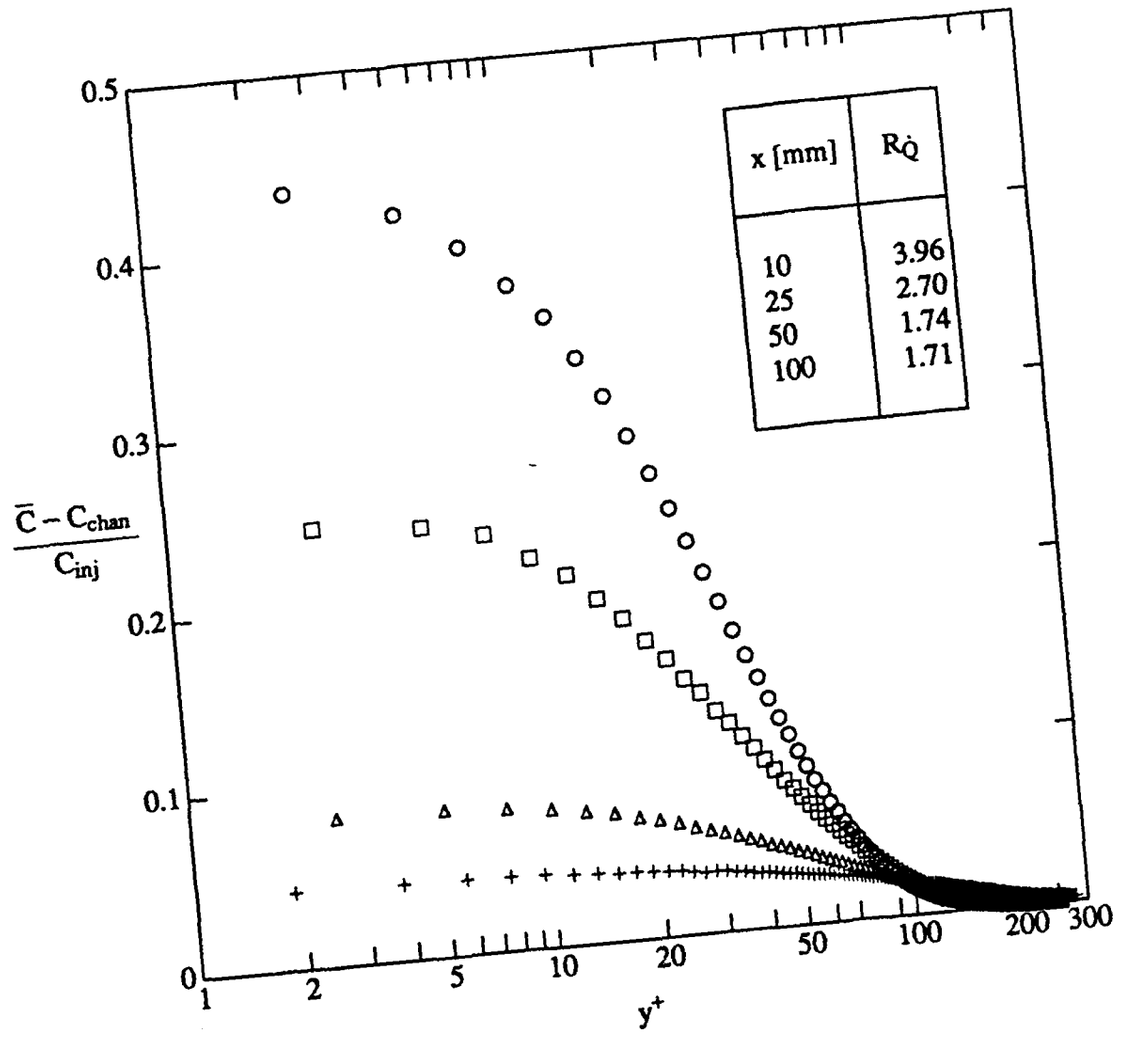

Figure 3.2: Effect of downstream location on mean concentration for water-injected flow; ○ - x=10 mm; □ - x=25 mm; △ - x=50 mm; + - x=100 mm;

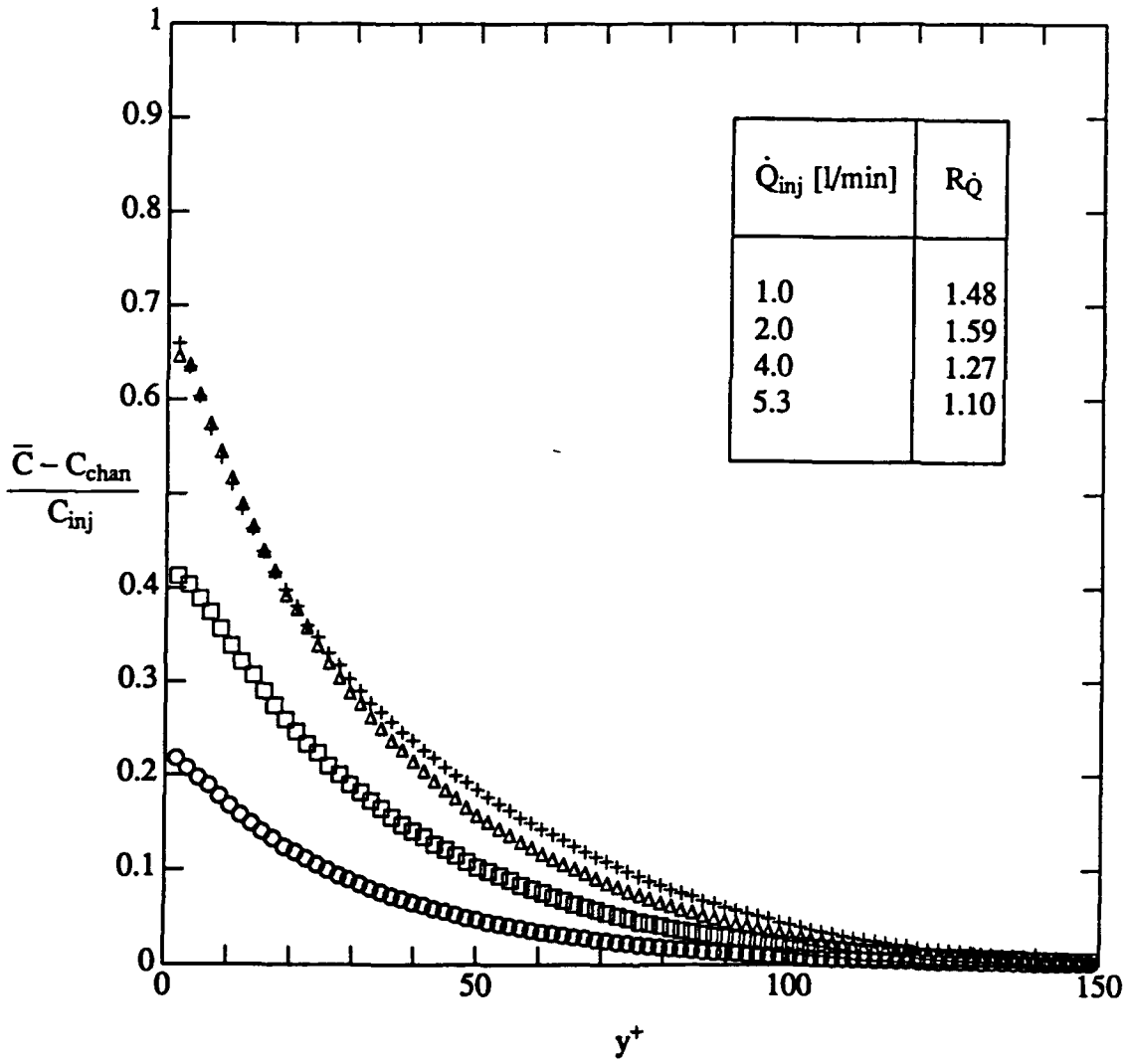

Figure 3.3: Effect of injector flow rate on mean concentration for water-injected flow at x=25 mm downstream of the injector slot; o - $\dot{Q}_{inj}$ = 1 l/min; □ - $\dot{Q}_{inj}$ = 2 l/min; Δ - $\dot{Q}_{inj}$ = 4 l/min; + - $\dot{Q}_{inj}$ = 5.3 l/min.

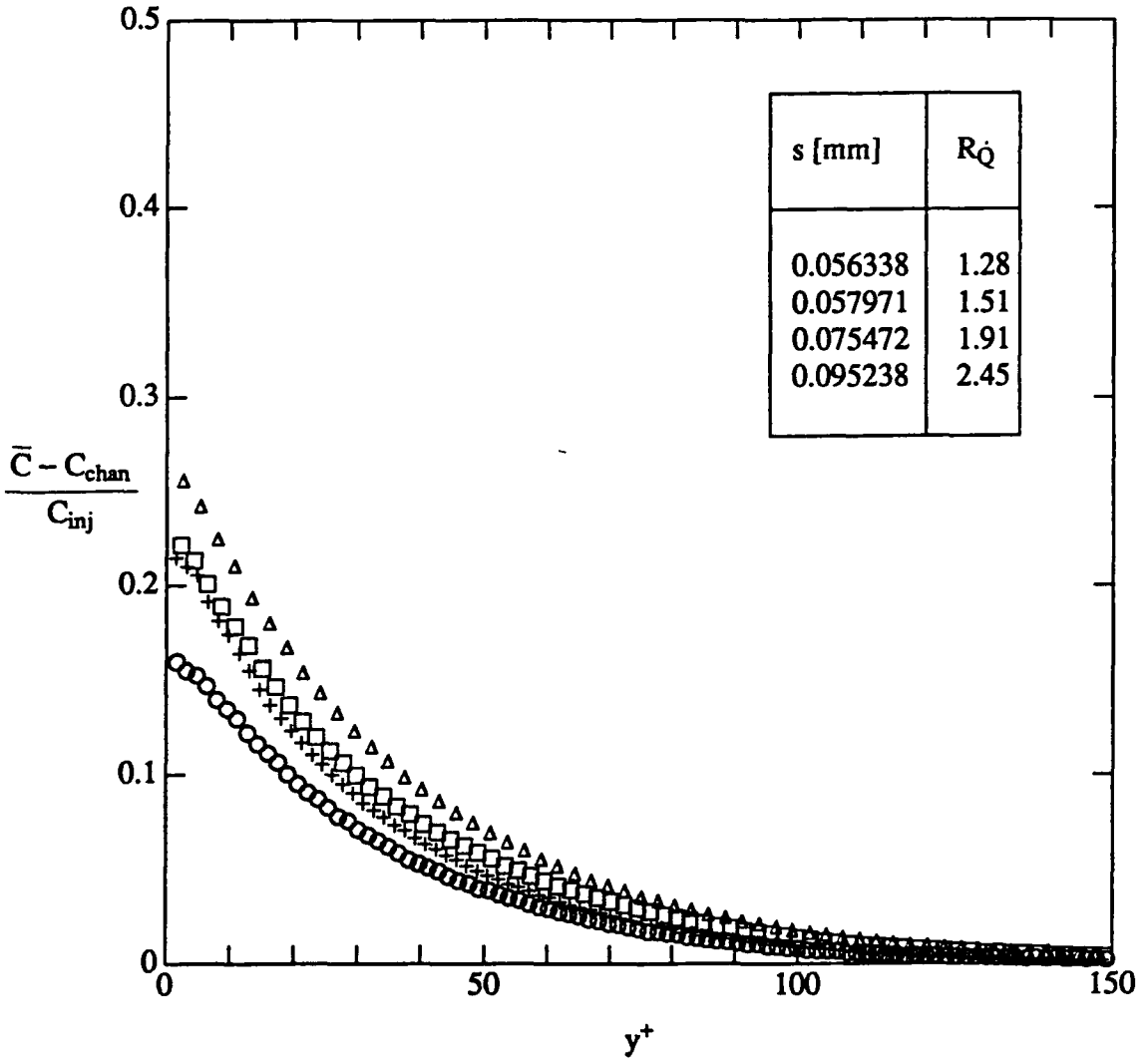

Figure 3.4: Effect of magnification factor on mean concentration for water-injected flow at x=25 mm downstream of the injector slot; o - s=0.056338 mm; □ - s=0.075472 mm; ∆ - s=0.095238 mm; + - 0.057971 mm.

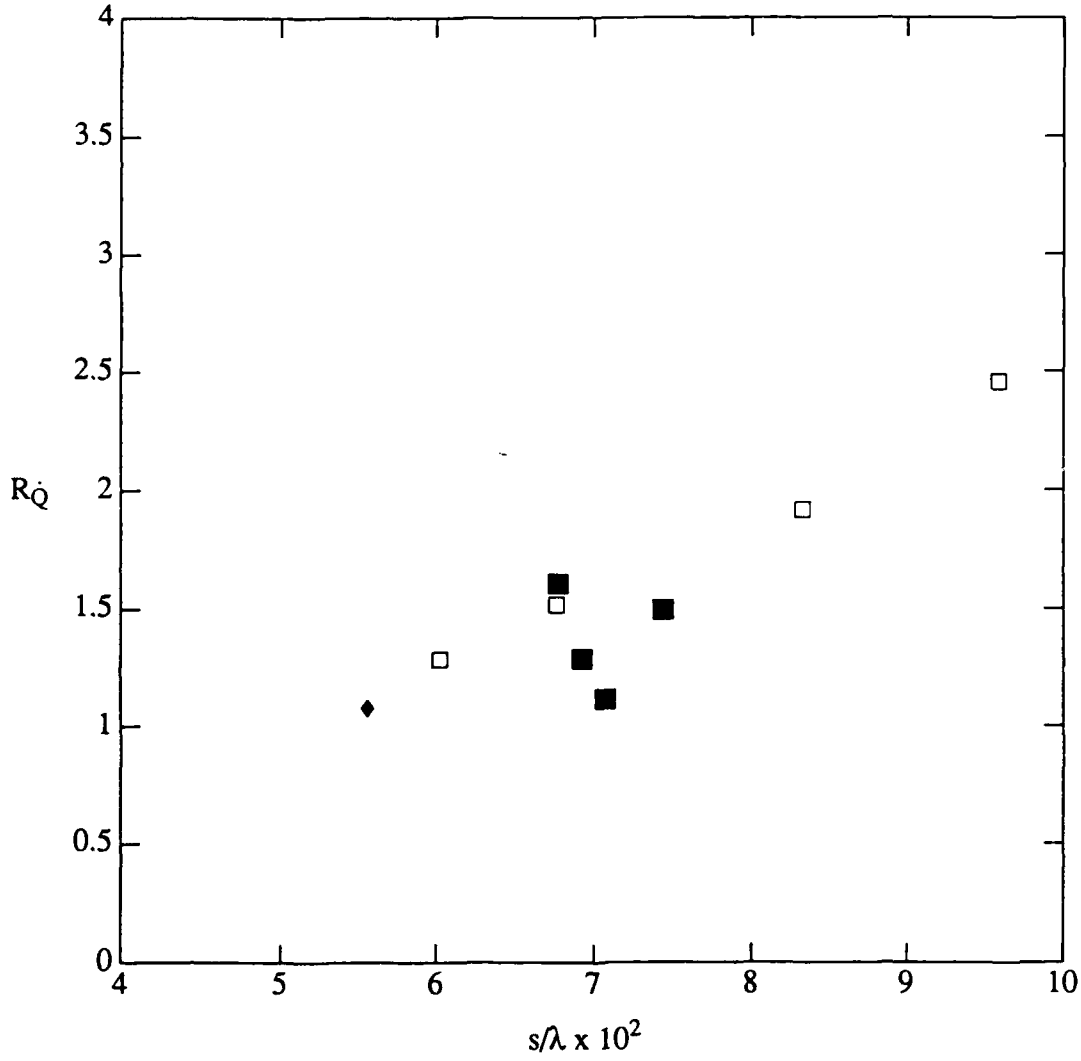

Figure 3.5: Effect of normalized photo-diode spacing on the mass flux ratio; □ - x=25 mm, injector fluid: water (variable magnification factor); ■ - x=25 mm, injector fluid: water (variable injection flow rate); ♦ - x=620 mm in zero pressure gradient boundary layer, injector fluid: 1000 ppm AP273 (data by J.E. Koskie, 1991).

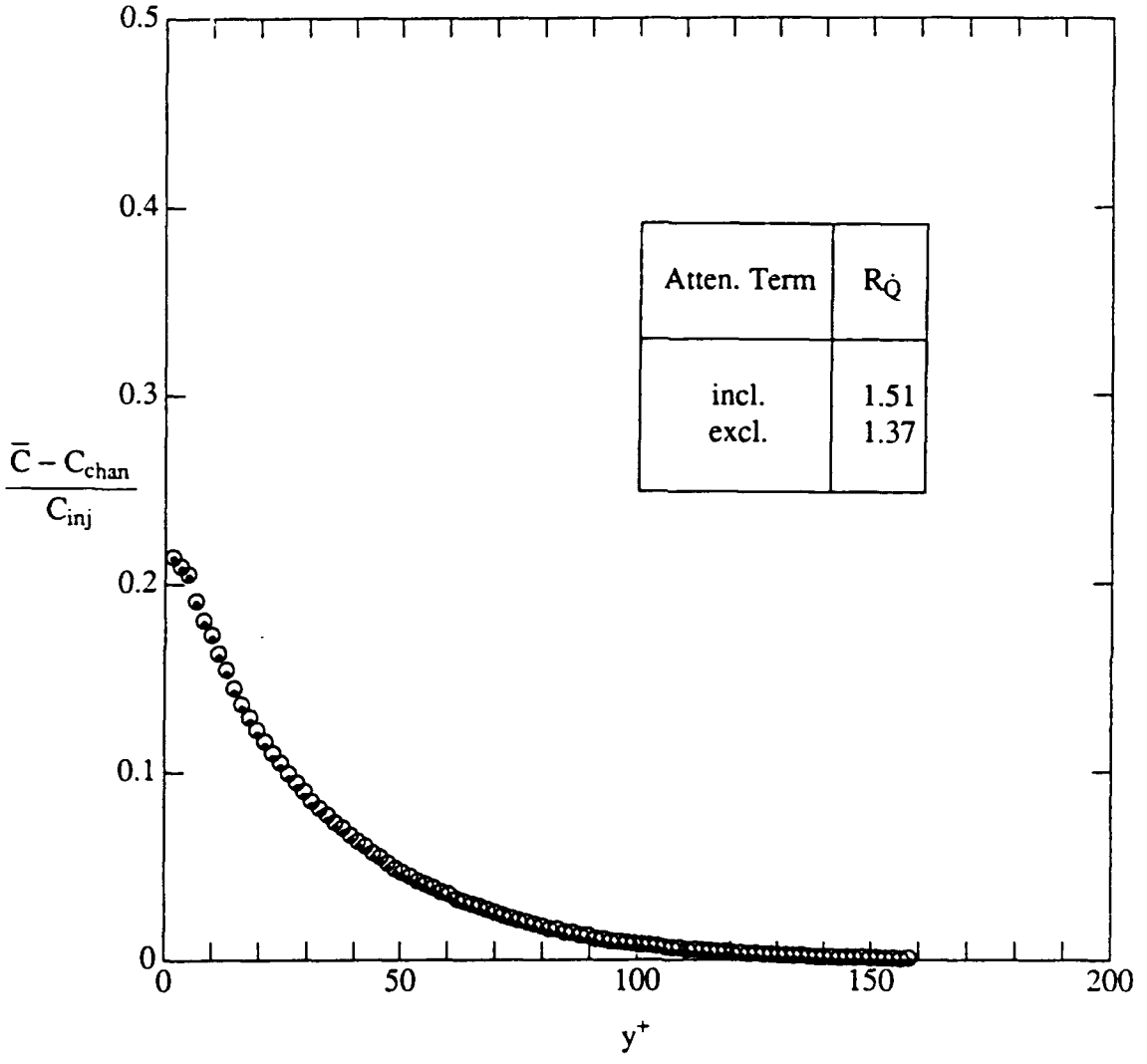

Figure 3.6: Inner normalized plot of mean concentration for water-injected flow at x=25 mm downstream of the injector slot showing the influence of the attenuation factor; o - including attenuation term; • - excluding attenuation term.

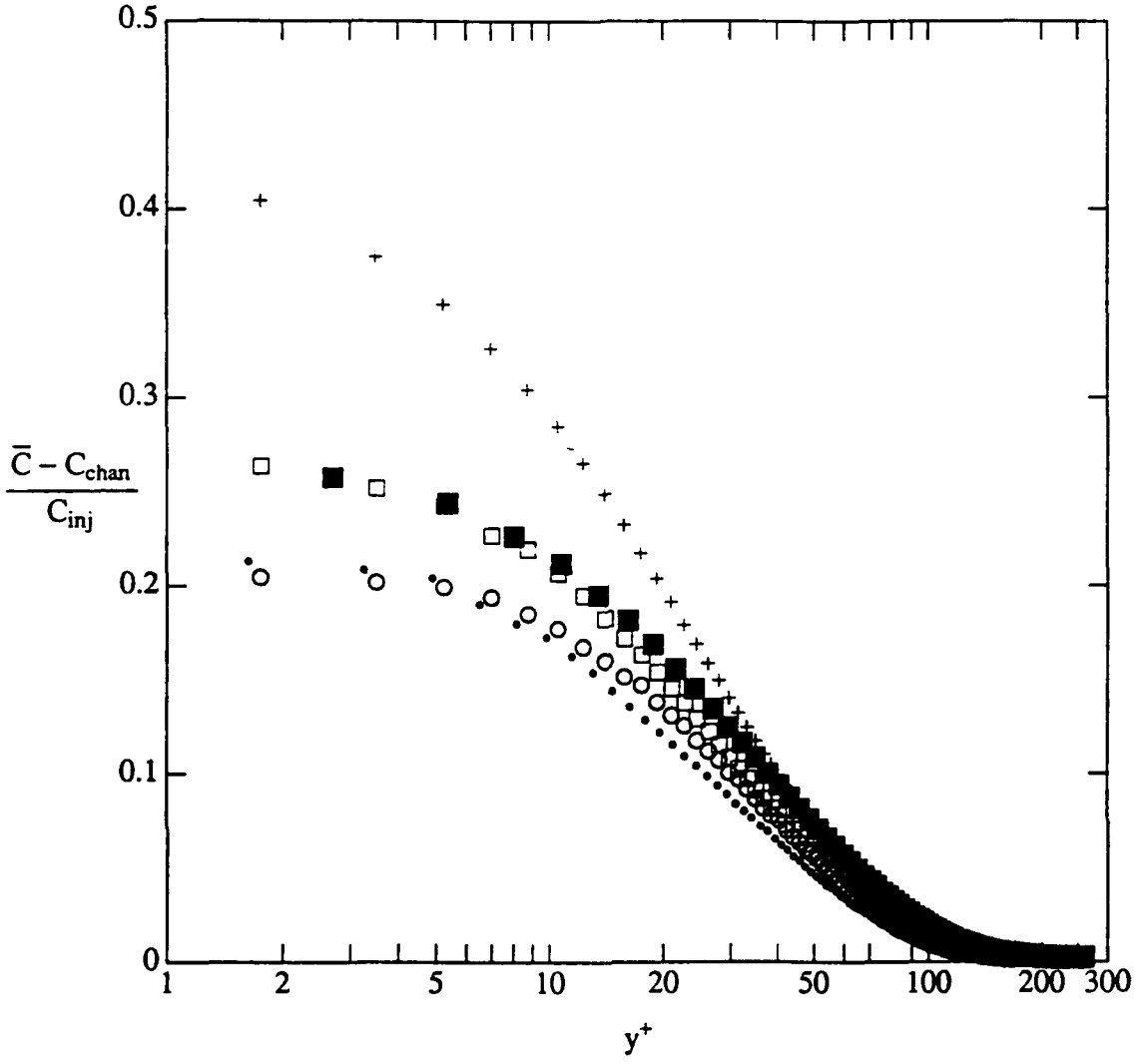

Figure 3.7: Inner normalized plot of mean concentration for water-injected flow at x=25 mm downstream of the injector slot for different experimental parameters as shown in the Table.

Symbol	$\overline{V}_{inj}$	$R_{\dot{Q}}$	s [mm]	T_s [msec]	P_{Las} [mW]
o	0.35	2.19	0.06173	0.333	50
•	0.45	1.51	0.05797	0.333	100
□	0.66	2.25	0.06173	0.500	80
■	0.75	2.45	0.09524	0.333	100
+	1.61	3.10	0.06173	1.000	110

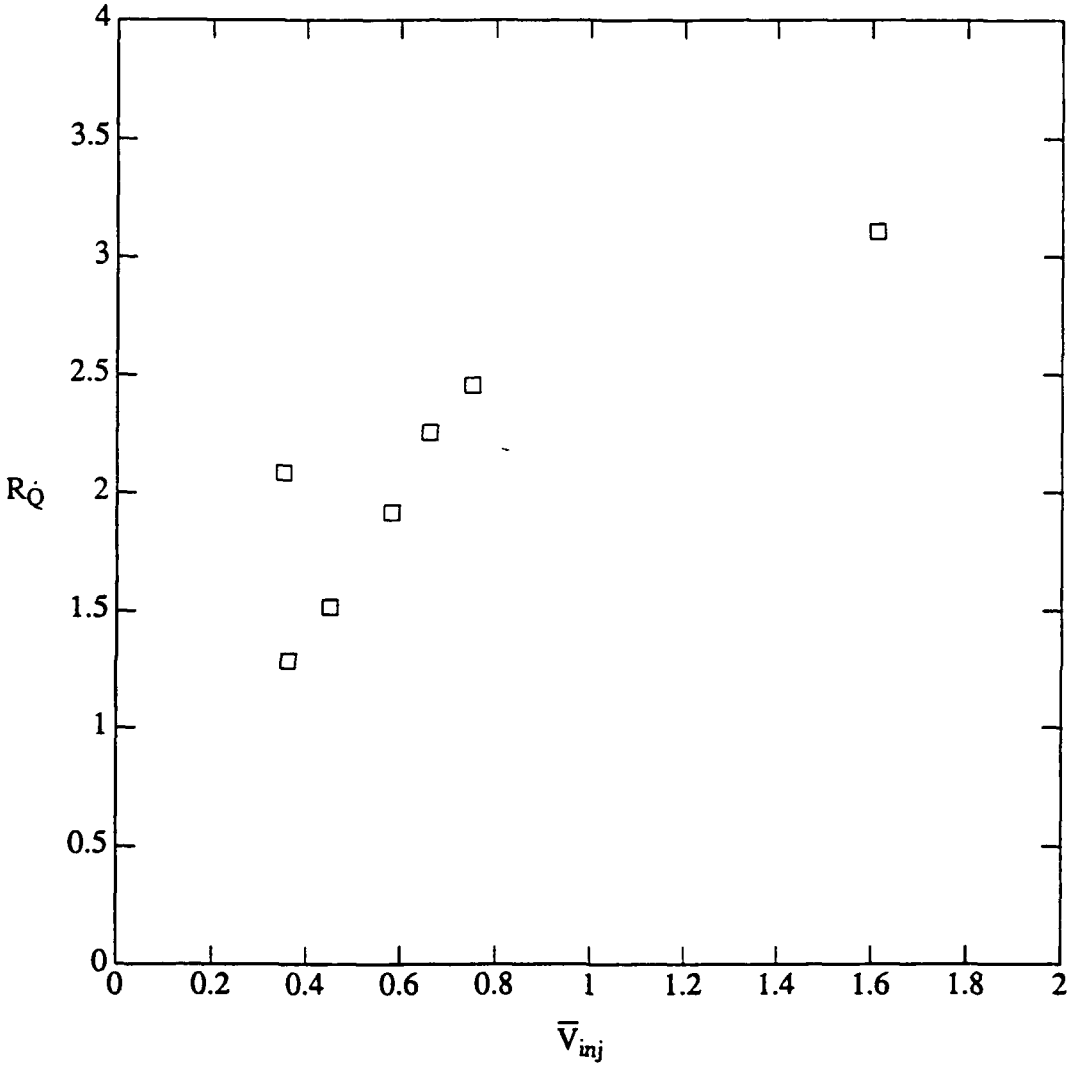

Figure 3.8: Effect of average array voltage on mass flux ratio.

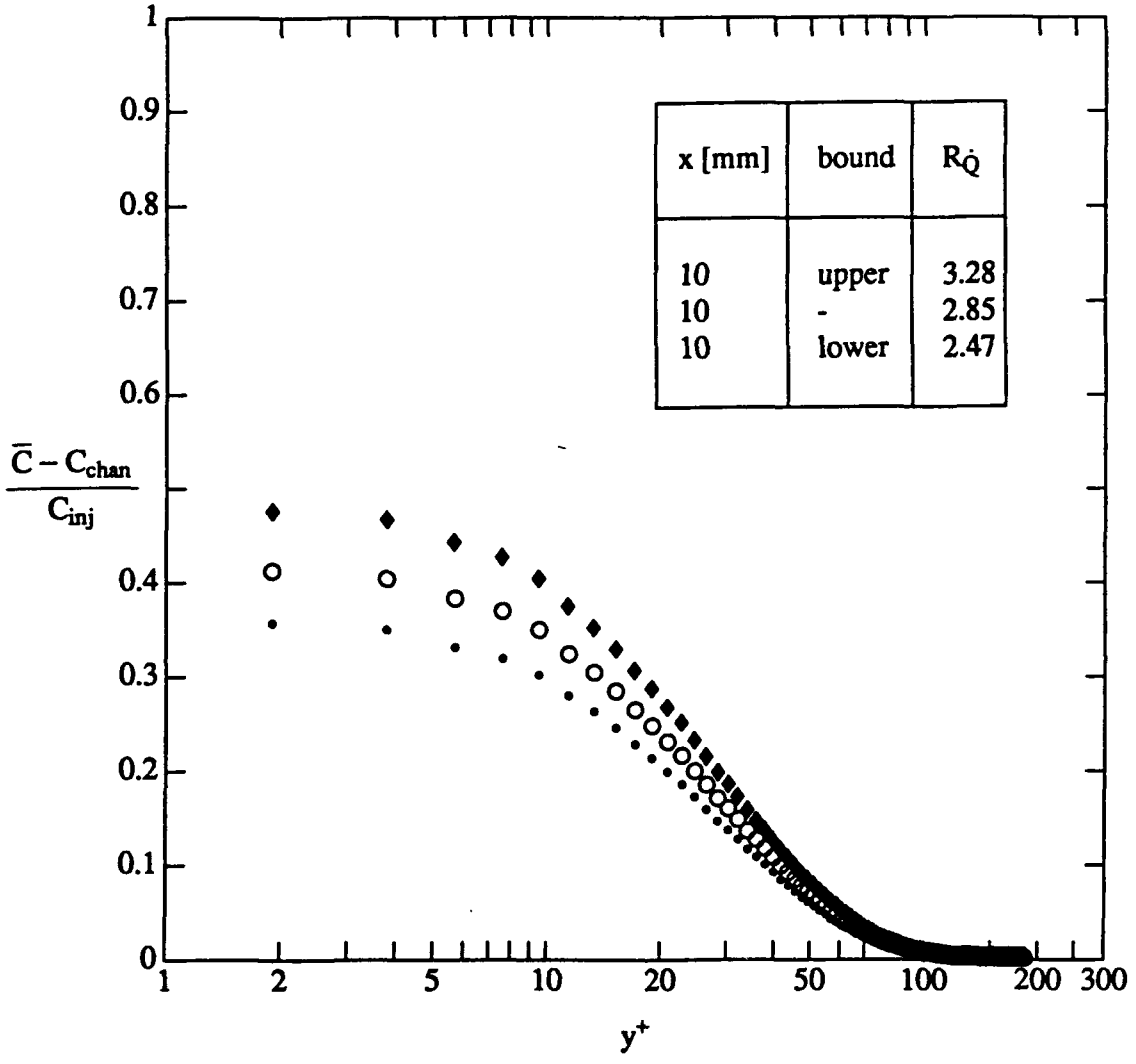

Figure 3.9: Inner normalized plot of mean concentration for water-injected flow at x=10 mm downstream of the injector slot showing the estimated 95% uncertainty limits; o - x=10 mm; • - x=10 mm (lower error bound); ♦ - x=10 mm (upper error bound).

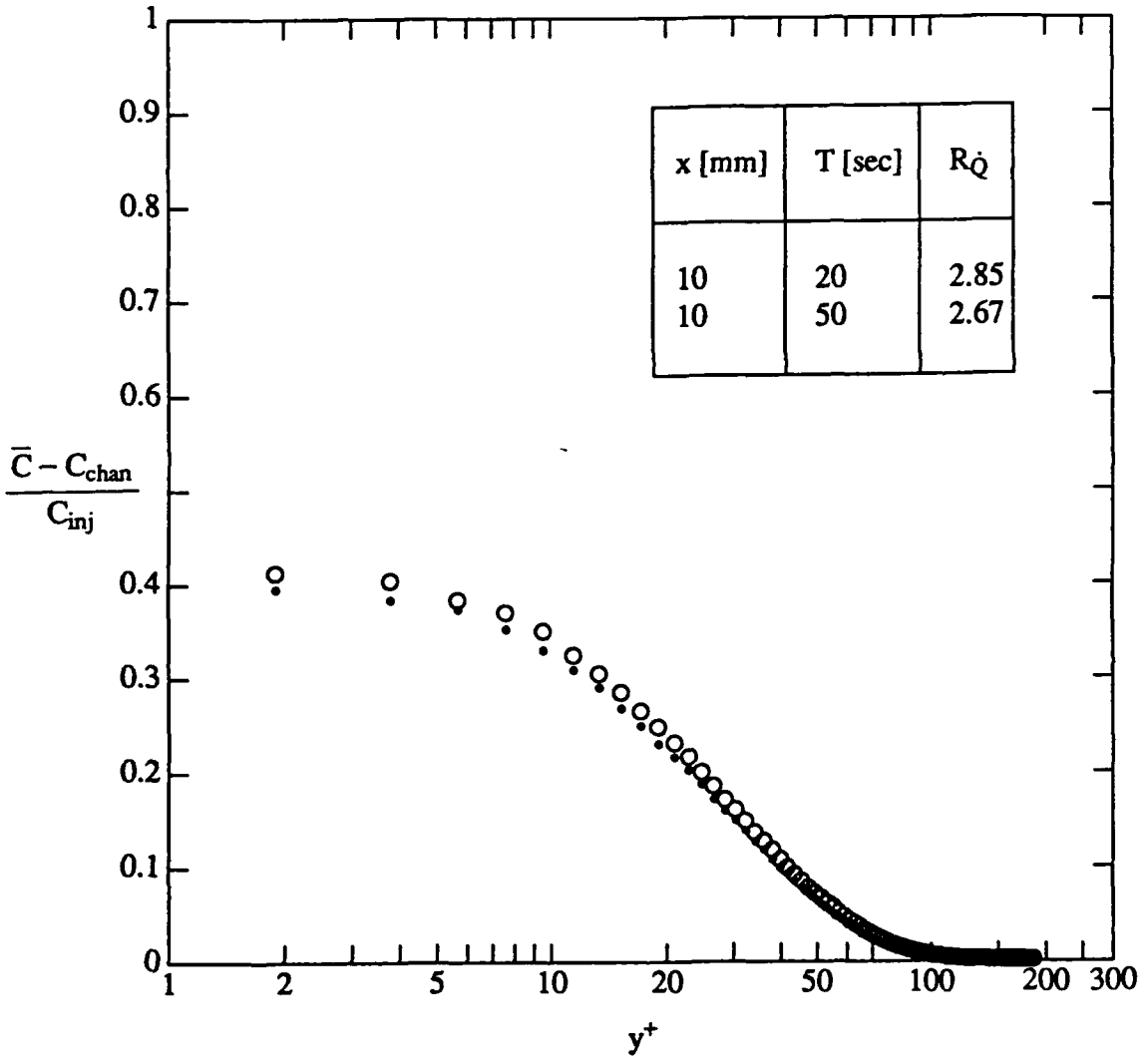

Figure 3.10: Effect of integration time on mean concentration for water-injected flow at x=10 mm downstream of the injector slot; o - T=20 sec; • - T=50 sec.

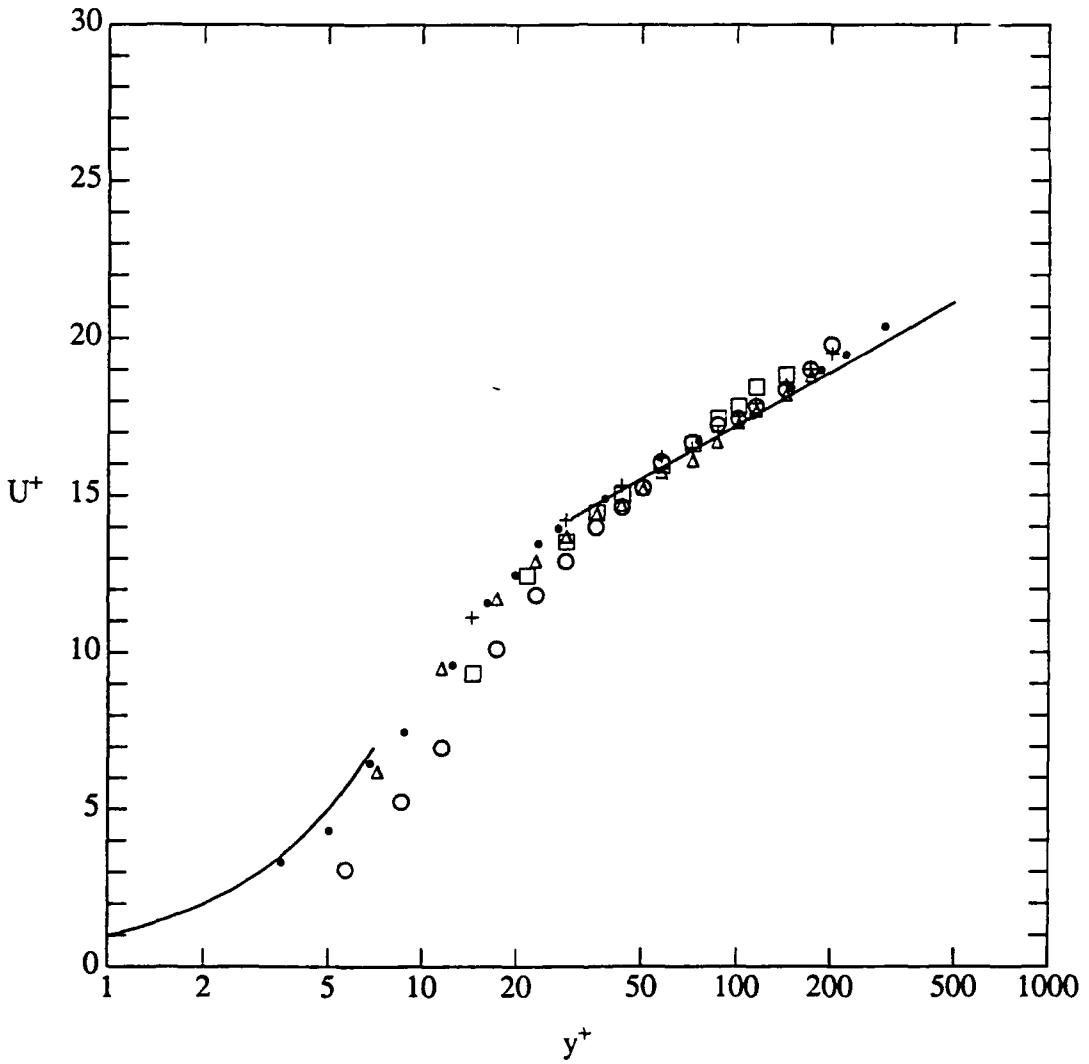

Figure 3.11: Inner normalized plot of mean streamwise velocity in channel flows without injection and with water injection; • - no injection; ○ - x=10 mm; □ - x=25 mm; △ - x=50 mm; + - x=100 mm.

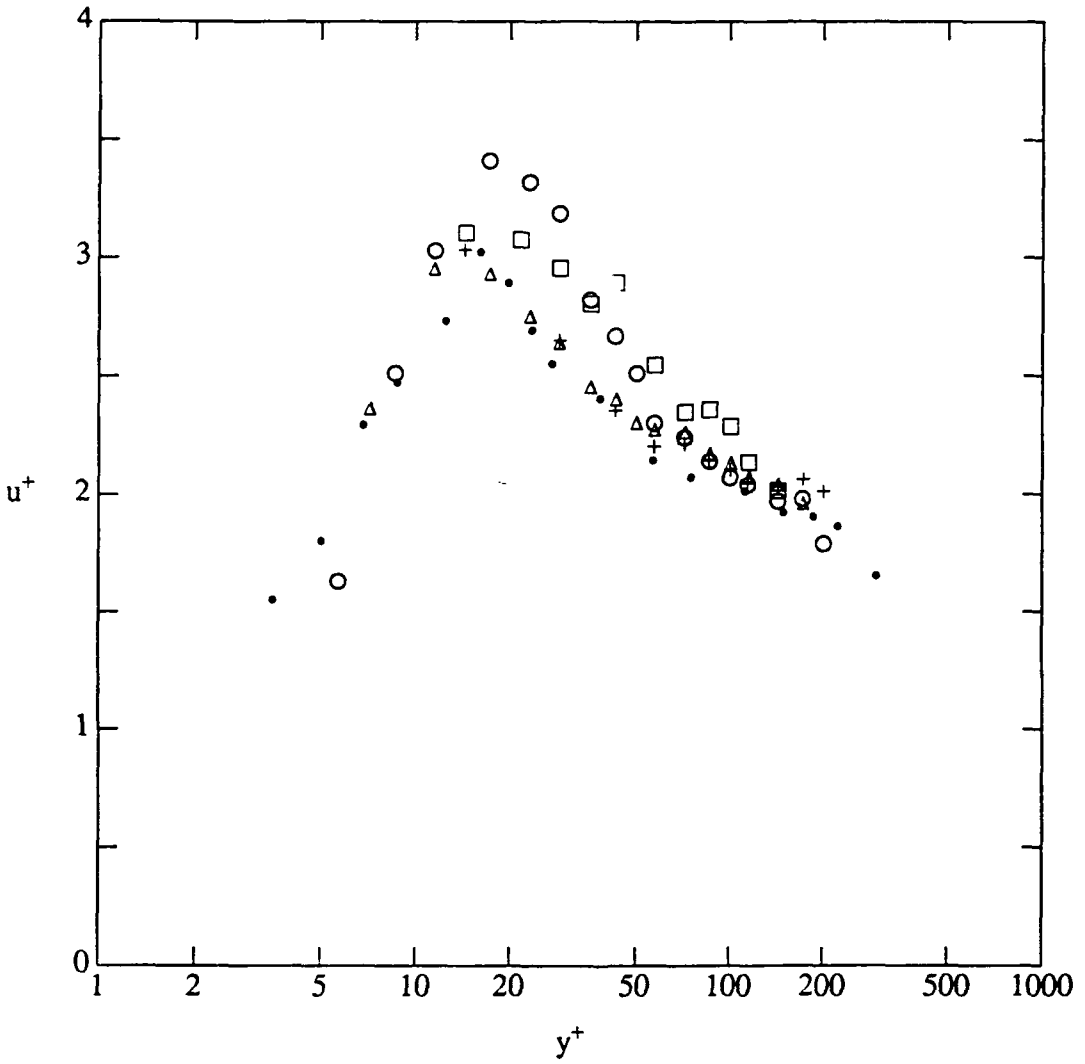

Figure 3.12: Variation of root-mean-square streamwise velocity fluctuation with distance from the wall in channel flows without injection and with water injection; • - no injection; o - x=10 mm; □ - x=25 mm; Δ - x=50 mm; + - x=100 mm.

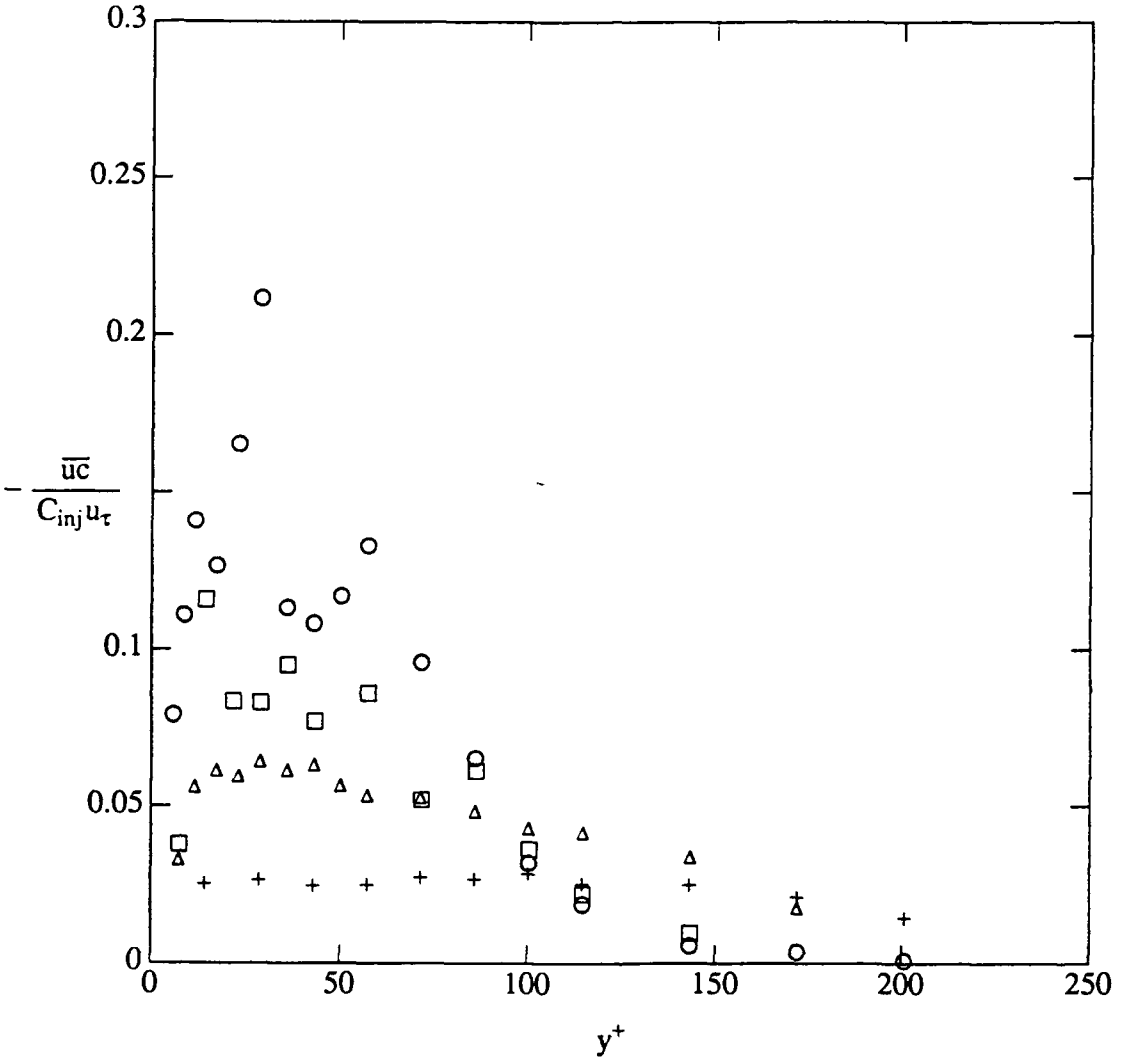

Figure 3.13: Turbulent streamwise mass transport for water-injected flow; o - x=10 mm; □ - x=25 mm; Δ - x=50 mm; + x=100 mm.

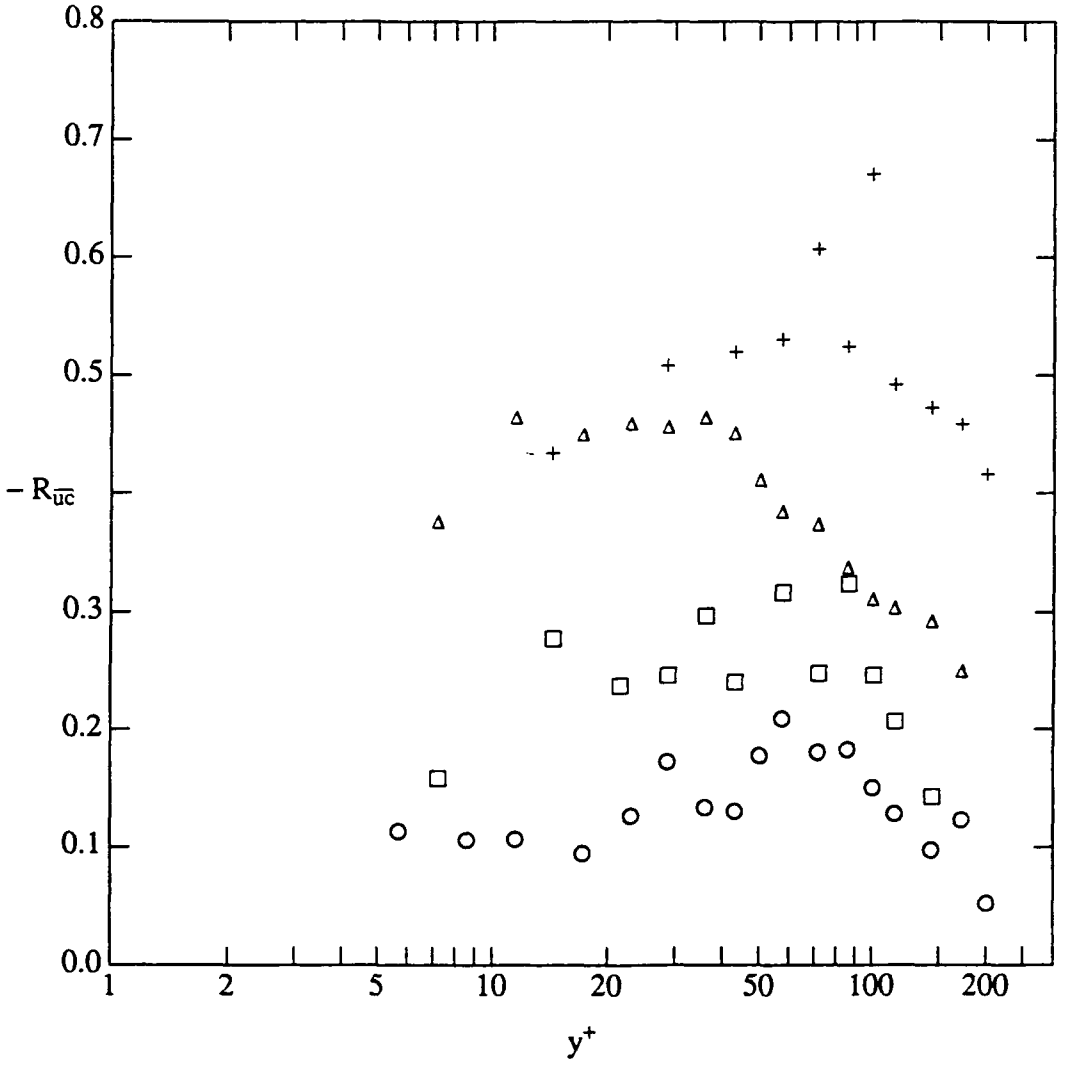

Figure 3.14: Streamwise mass-transport correlation coefficient for water injection; ○ - x=10 mm; □ - x=25 mm; △ x=50 mm; + - x=100 mm.

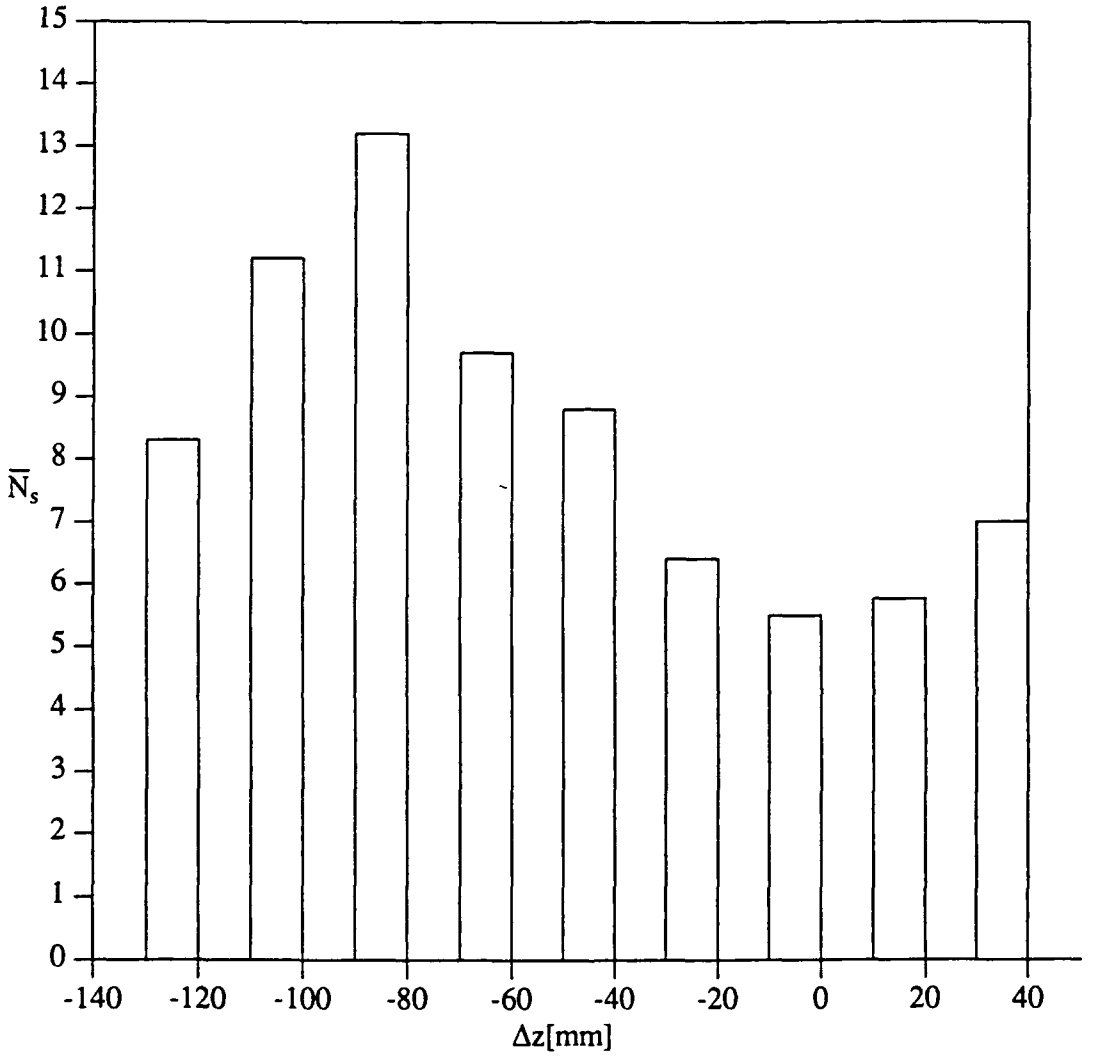

Figure 3.15: Histogram showing number of occurences of high concentration polymer streaks 100 mm downstream of the injector slot.

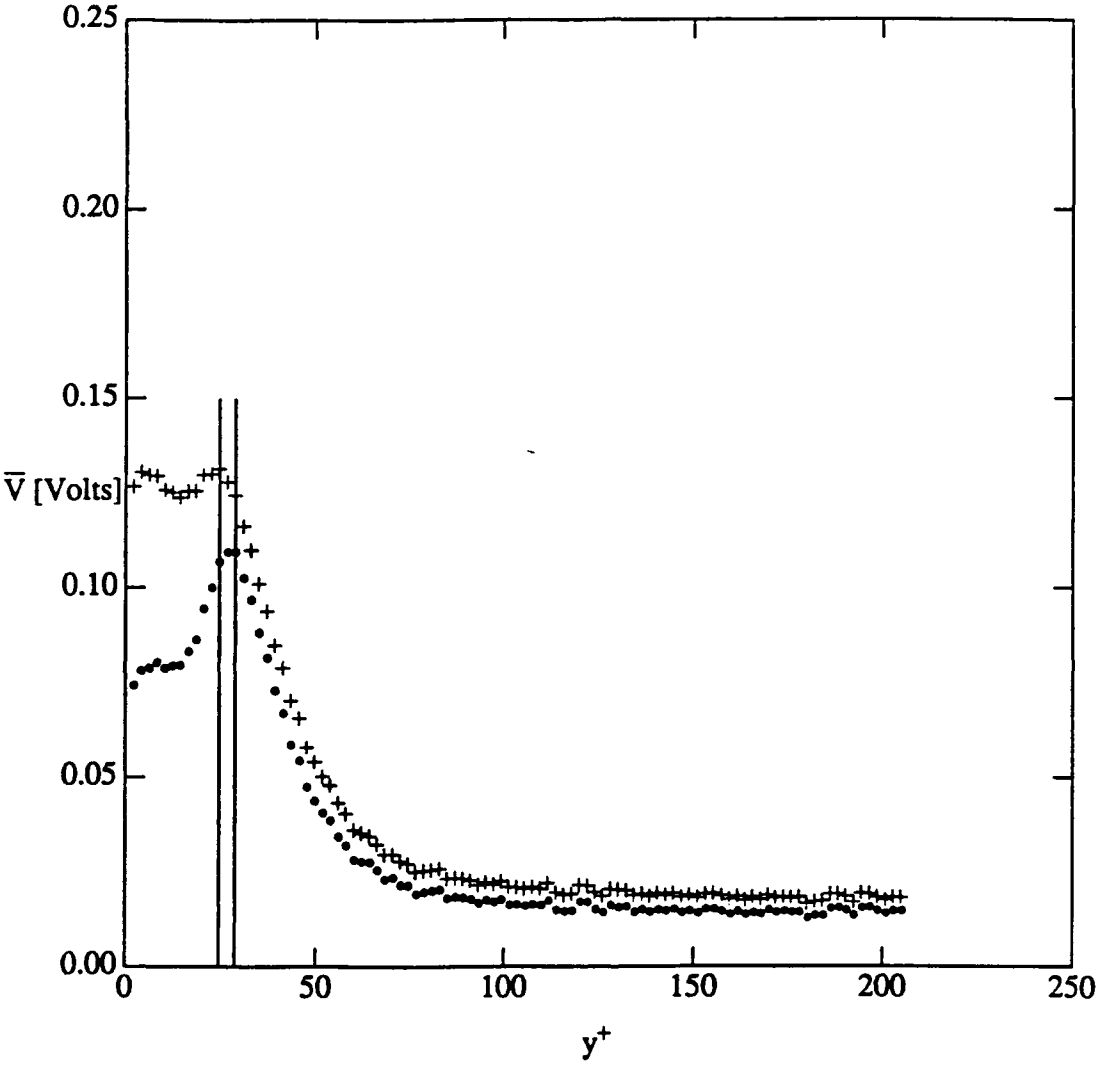

Figure 3.16: Mean voltage on line-scan camera array at x=25 mm and y=1.0 mm for • no injection and + during injection of undyed polymer solution (700ppm of AP273).

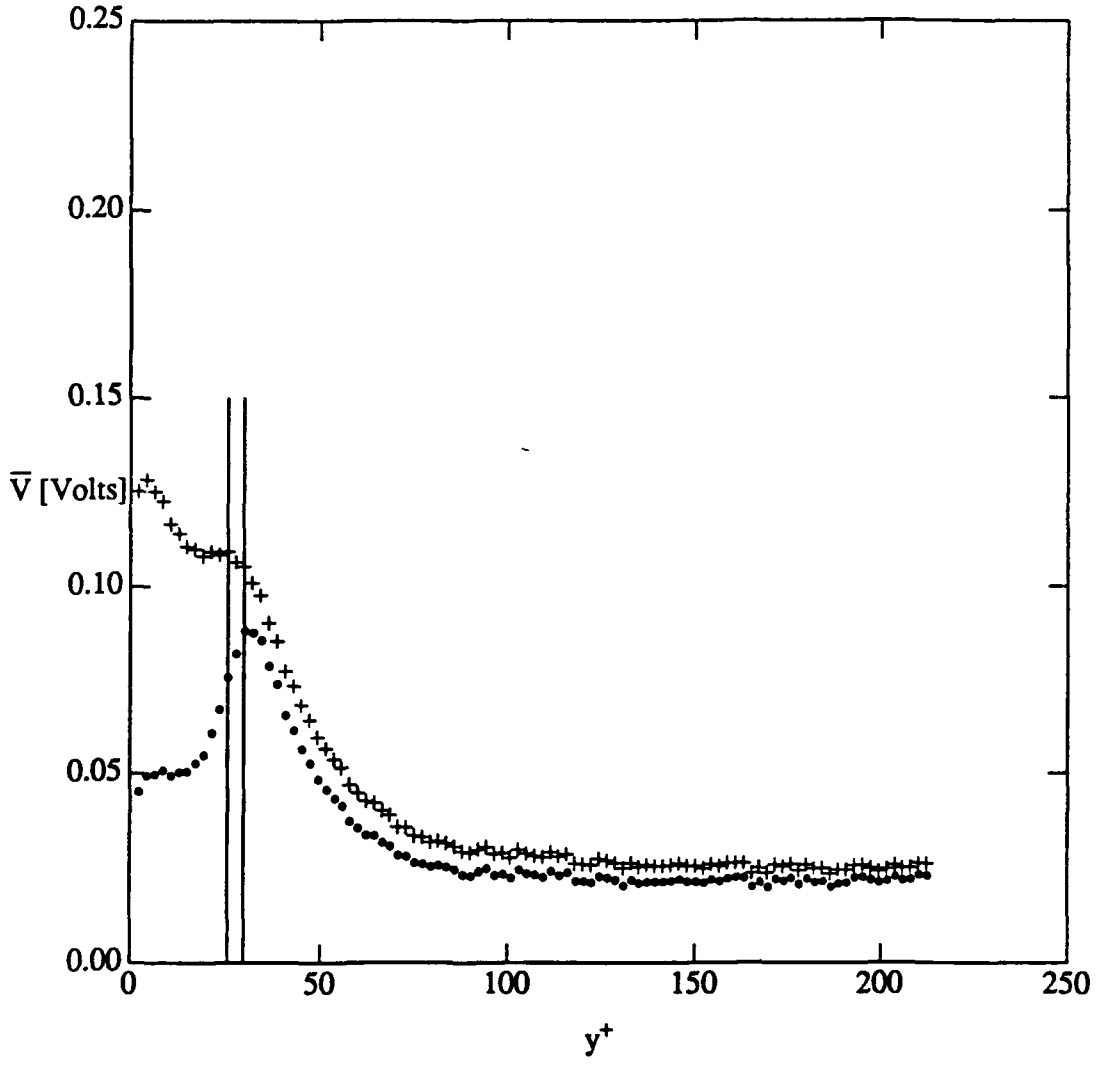

Figure 3.17: Mean voltage on line-scan camera array at x=100 mm and y=1.0 mm for • no injection and + during injection of undyed polymer solution (700ppm of AP273).

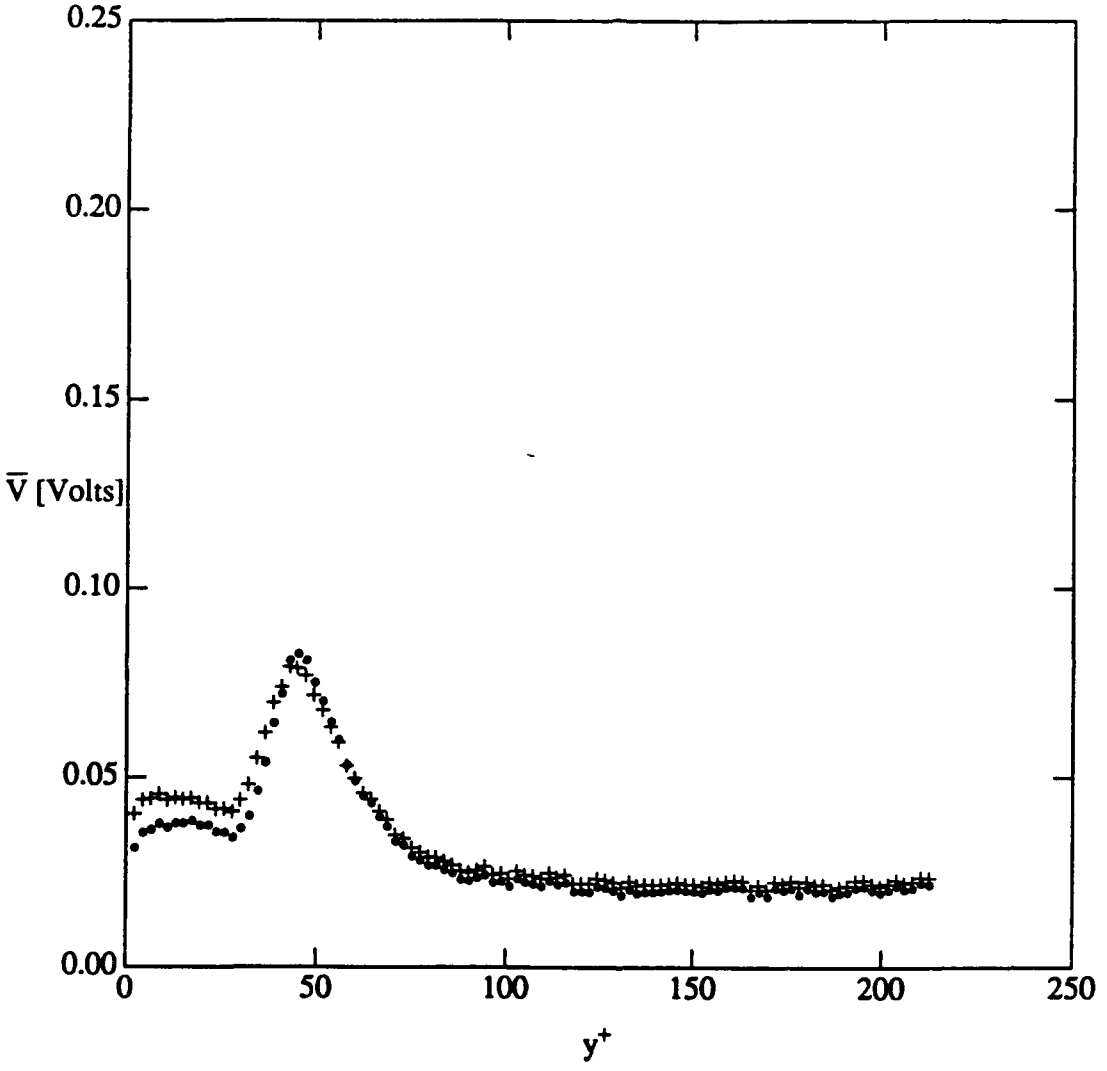

Figure 3.18: Mean voltage on line-scan camera array at x=100 mm and y=1.5 mm for • no injection and + during injection of undyed polymer solution (700ppm of AP273).

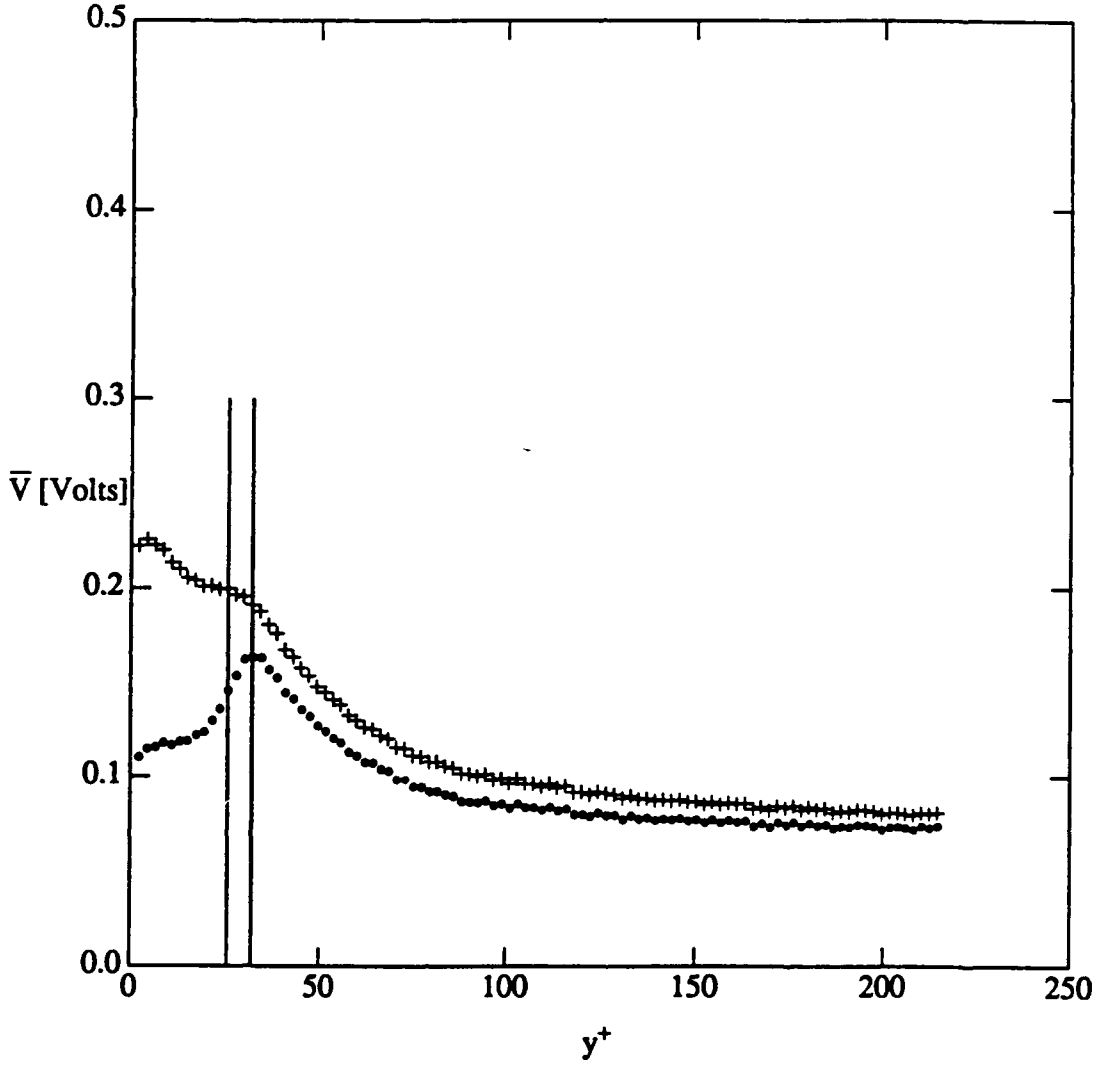

Figure 3.19: Mean voltage on line-scan camera array at x=100 mm and y=1.0 mm for • no injection and + during injection of dyed polymer solution (700ppm of AP273).

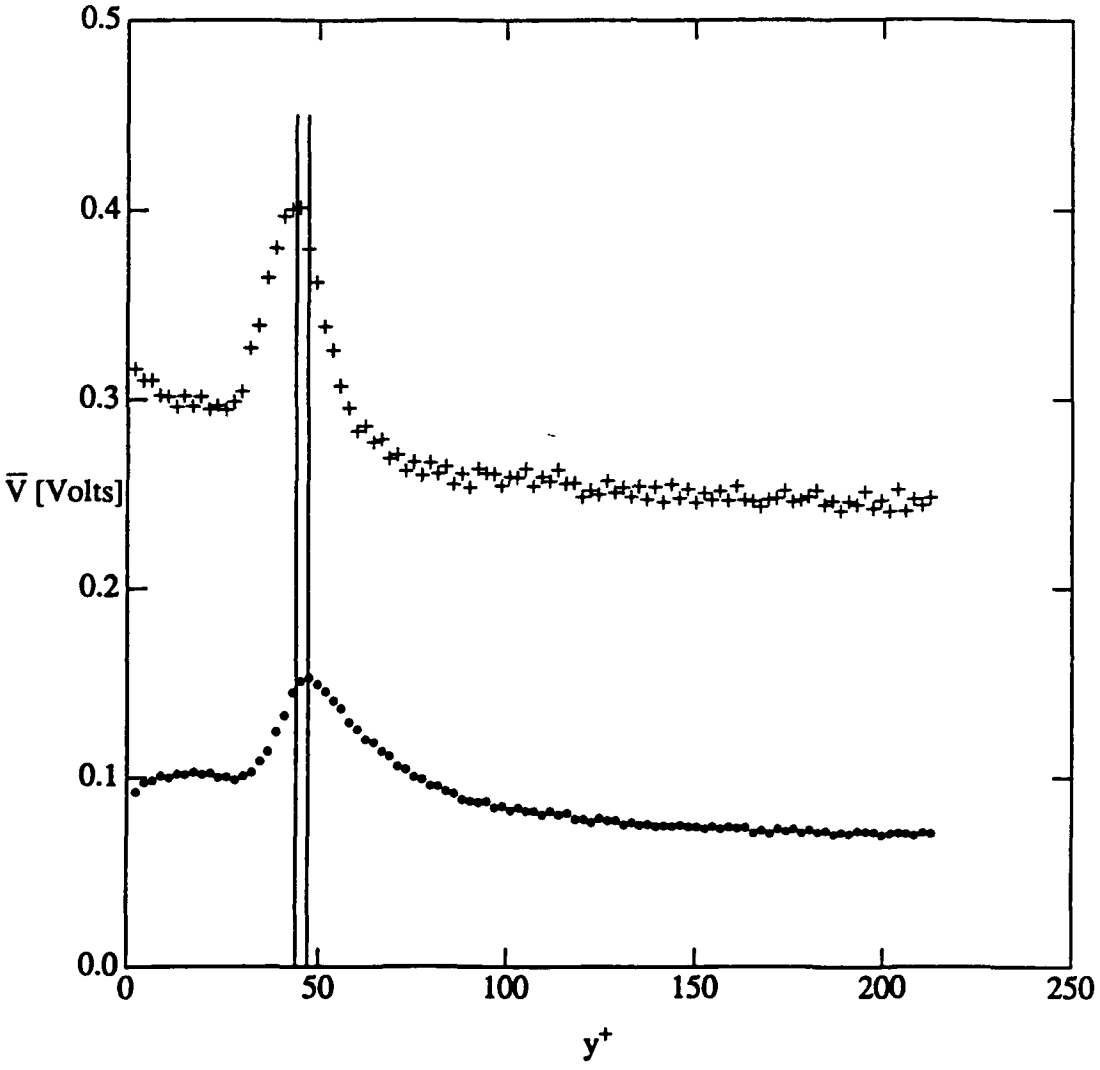

Figure 3.20: Mean voltage on line-scan camera array at x=100 mm and y=1.5 mm for • no injection and + during injection of dyed polymer solution (700ppm of AP273).

APPENDICES

Appendix A

In order to measure accurately the additive concentration using the laser-induced-fluorescence technique, the concentration of the injected fluid has to be represented by the concentration of the dye molecules. These tests were conducted to determine whether the fluorescence intensity of the dye was independent of the process by which the dye was mixed with the polymer solution. Two different methods were tested as mentioned earlier in Chapter 2. These will be referred to as the Penn State (PS) and the Purdue (PU) method.

In order to measure the fluorescence intensity as a function of dye concentration for different mixing procedures, a small test cell was constructed that allowed the passage of fresh dyed mixture through a flow channel that had a height of 1.59 mm (1/16 inch). The test cell was build out of acrylic with a glass window attached to its front to have optical access to the excitation beam (488 nm), which was oriented perpendicular to the main flow direction. The line-scan camera was aligned with the laser beam and the fluorescence intensity for a certain concentration was determined with an oscilloscope. In order to verify the procedure, water at different dye concentrations was used prior to the polymer mixtures. The results for all measurements are shown in Figure A.1. The ordinate was normalized with the intensity measured for a concentration of $C = 1$ ppm because the response varied for different runs due to fluctuations in the laser power and

different locations at which the laser beam entered the test cell. The different quality of the water was very sensitive to the fluorescence intensity of the dye which is the main reason for this choice of normalization.

The main trend of the data shows that the response of the dye molecule for different dye concentrations does not depend on the mixing procedure of the solvent (water or polymer solution) with the fluorescein dye. In fact, the fluorescence intensity is linearly dependent on the the dye concentration which was expected. The main result of this test was that the behavior of the dye molecule did not alter with respect to whether the dye was mixed with the polymer immediately before the experiment (PU method) or whether it was given time to hydrate with the polymer solution (PS method).

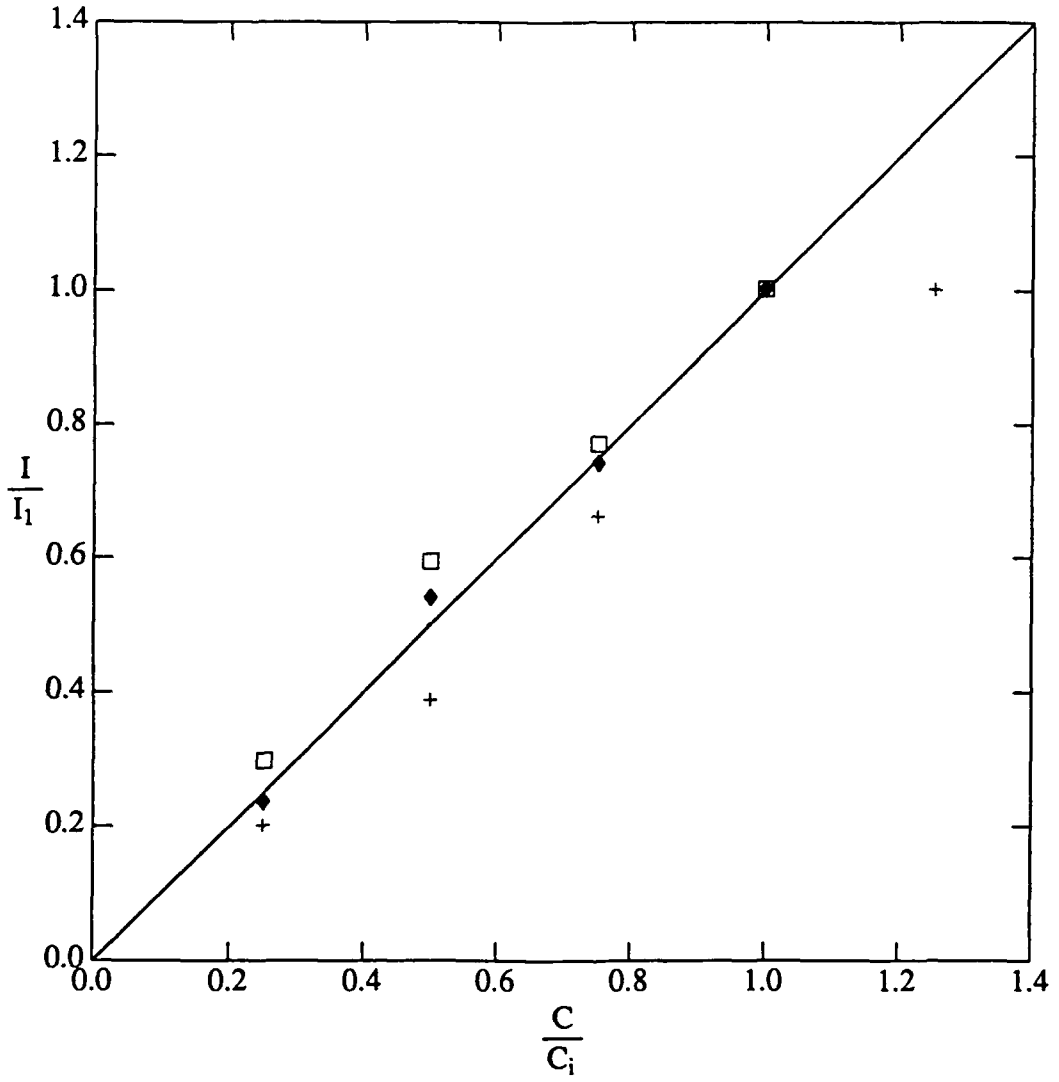

Figure A.1: Fluorescence intensity as a function of dye concentration. ♦ - Water; □ - Polymer PU; + - Polymer PS.

Appendix B

In this part of the report, an additional set of injection experiments will be documented. In these tests, the scan frequency which is the inverse of the array exposure time has been changed between the calibration procedure and the injection experiment in order to keep the array voltages within the desired range. Four different mean concentration profiles are shown in Figure B.1 where the scan frequency for the calibration procedure was varied between 500 Hz and 3,000 Hz while it was held constant at 3,000 Hz during the injection of dyed water. The results shown in the plot indicate that there is a problem associated with different exposure times. It is not clear at this point whether the apparent offset in the concentration values far away from the wall can be attributed to an error in the implementation of the working equation in the data reduction program.

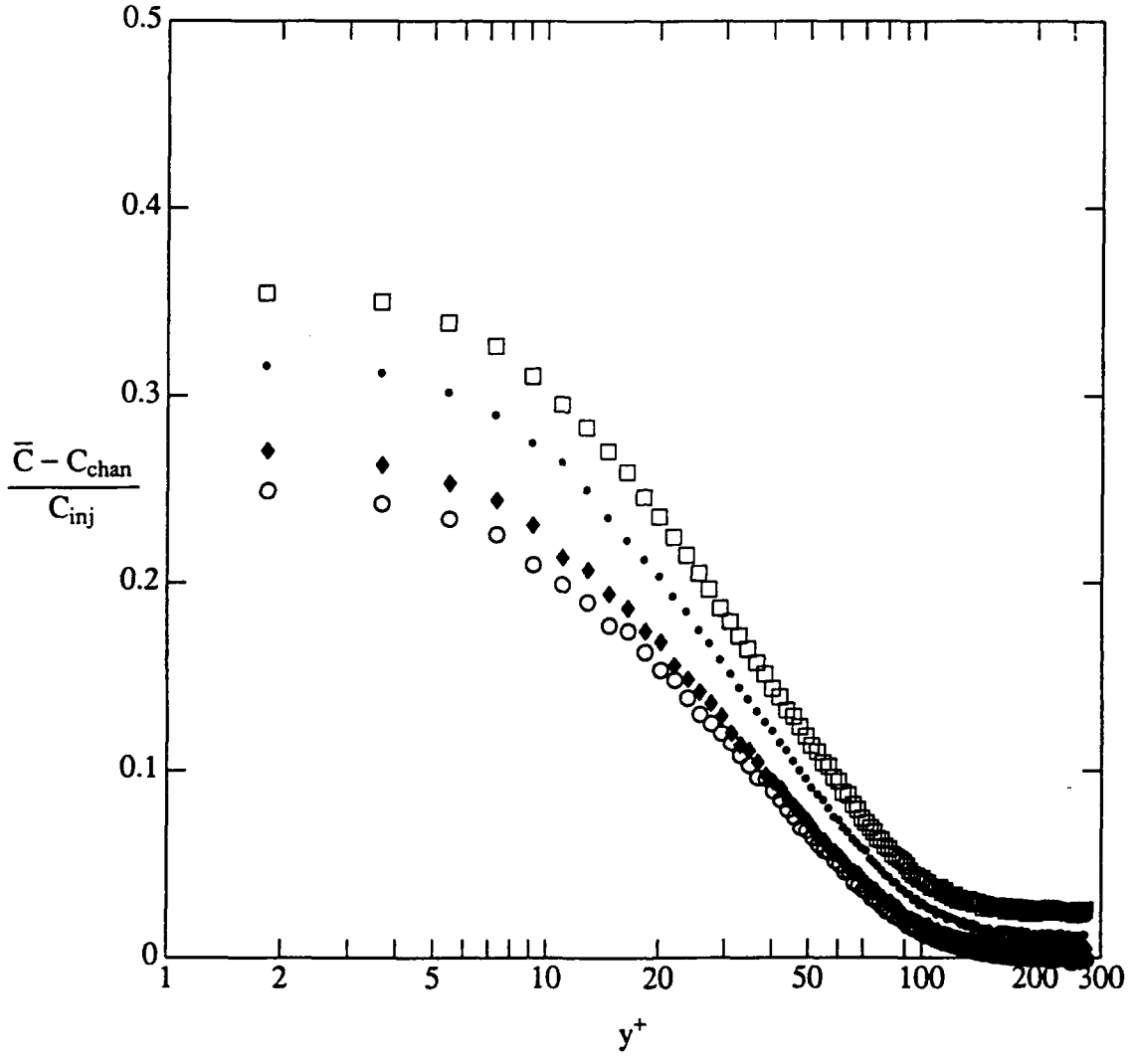

Figure B.1: Effect of exposure time on mean concentration for water-injected flow at x=25 mm downstream of the injector slot; ○ - $f_{sc,off}$ = 3,000 Hz and $f_{sc,inj}$ = 3,000Hz, □ - $f_{sc,off}$ = 500 Hz and $f_{sc,inj}$ = 3,000Hz, • - $f_{sc,off}$ = 1,000 Hz and $f_{sc,inj}$ = 3,000Hz, ♦ - $f_{sc,off}$ = 1,500 Hz and $f_{sc,inj}$ = 3,000Hz.